www.acsnano.org

Moiré Patterns in 2D Materials: A Review

Feng He,[*,⊥] Yongjian Zhou,[⊥] Zefang Ye, Sang-Hyeok Cho, Jihoon Jeong, Xianghai Meng, and Yaguo Wang[*]

Cite This: https://doi.org/10.1021/acsnano.0c10435

ABSTRACT: **Quantum materials have attracted much attention in recent years due to their exotic and incredible properties. Among them, van der Waals materials stand out due to their weak interlayer coupling, providing easy access to manipulating electrical and optical properties. Many fascinating electrical, optical, and magnetic properties have been reported in the moiré superlattices, such as unconventional superconductivity, photonic dispersion engineering, and ferromagnetism. In this review, we summarize the methods to prepare moiré superlattices in the van der Waals materials and focus on the current discoveries of moiré pattern-modified electrical properties, recent findings of atomic reconstruction, as well as some possible future directions in this field.**

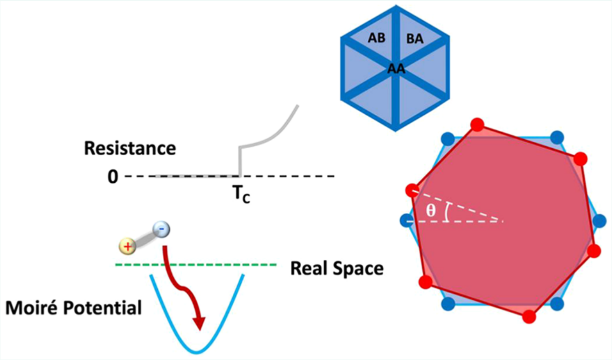

KEYWORDS: *atomic reconstruction, moiré superlattice, van der Waals materials, moiré exciton, unconventional superconductivity, unconventional ferroelectricity, magnetism, domain walls, hydrostatic pressure, mechanical strain*

INTRODUCTION

van der Waals (vdW) materials, including graphene, hexagonal boron nitride (hBN), and transition metal dichalcogenides (TMDCs), have been studied extensively during the past 10 years.[1−12] Many applications have emerged in recent years.[13−17] Although a different periodicity, *e.g.*, moiré pattern or moiré superlattice, was observed in a bilayer graphene system in 2013,[18] few works have focused on the properties associated with moiré patterns until recently, where strongly correlated regimes have been discovered with such periodicity,[19−22] leading to some emergent and intriguing properties, such as unconventional superconductivity,[23] topological conducting channels,[24−26] and exceptional optoelectronic behaviors.[24,27,28]

Here, we focus on the moiré patterns in which a large periodicity appears. The superposition of two similar layers will give rise to a different periodicity, e.g., moiré pattern or moiré superlattice. The difference in lattice constants,[28] translational shifts,[18,29] or the twisted angles[24,25,30−34] between two layers can change the periodicity of the moiré superlattice. Recently, Mason *et al.* even found that a moiré superlattice can form when assembling 2D materials on top of periodic dielectric substrates.[35−37]

Despite the rigid model assumption used for most discoveries, recent findings show that atomic reconstruction is important at small twisted angles and can alternatively explain some emergent phenomena.[25,31,32,38]

Understanding the physics behind the emergent properties driven by the formation of moiré patterns in 2D materials is both of scientific interest and application importance. In this review, we will summarize the methods to produce moiré patterns in 2D materials,[39−42] identify the twisted angles,[42−44] the current discoveries of electrical properties modified by moiré pattern, such as moiré excitons,[45−48] superconductivity,[21,23,49] and ferromagnetism,[50] current findings of atomic reconstruction,[25,31,32,38] as well as some possible future directions in this field.

HOW TO PREPARE MOIRÉ PATTERN SAMPLES

In this section, we will introduce the existing stacking configurations depending on twisted angles in the case of graphene and TMDC[18,40] and present the ways to realize a moiré superlattice with graphene and TMDCs to characterize its twisted angles. The methods to prepare moiré patterns include the vdW transfer technique,[40,51] the plasmon-enhanced chemical vapor deposition (PE-CVD) method,[42] and imple-

Received: December 14, 2020
Accepted: March 16, 2021

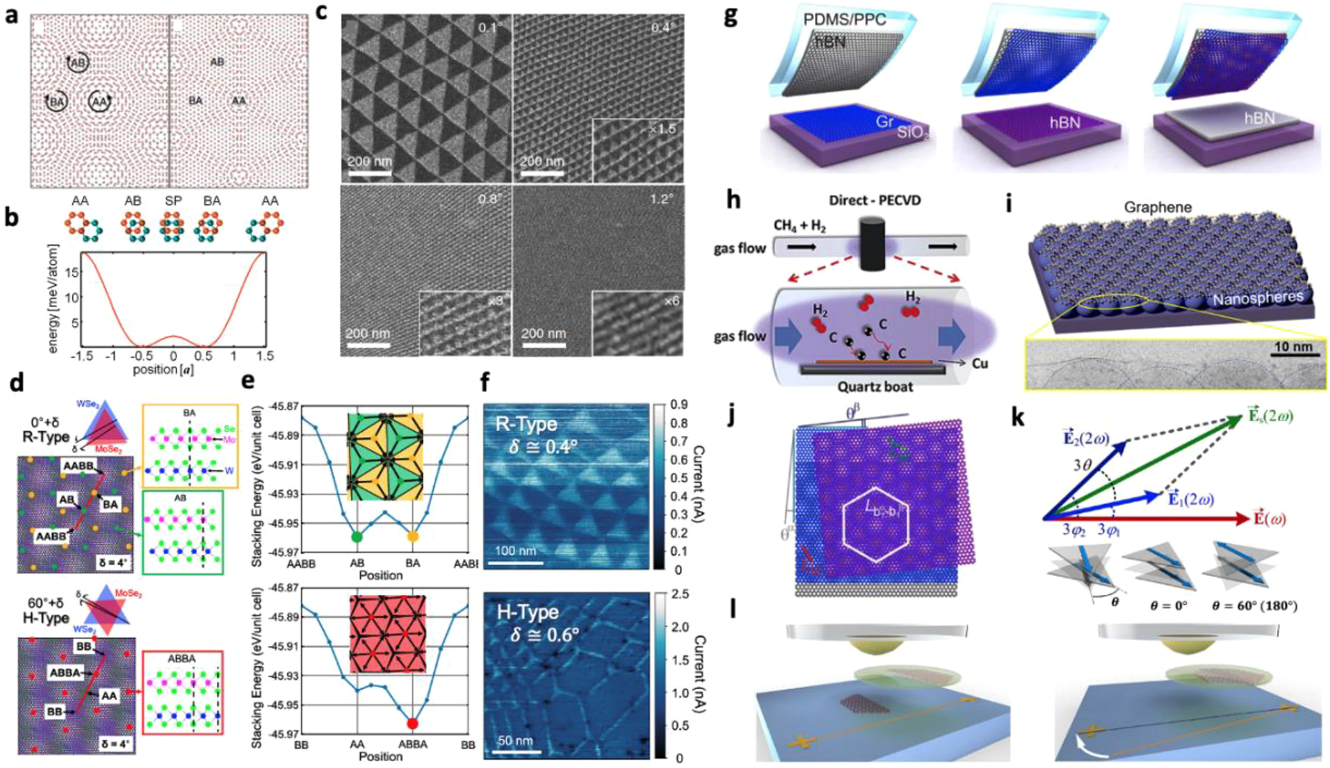

Figure 1. Characterization of the moiré pattern in vdW materials. (a) Schematics of twisted bilayer graphene (TBG) (left) before and (right) after the atomic reconstruction, with arrows representing rotational modulation.[32] Adapted with permission from ref 32. Copyright 2019 Springer Nature. (b) Energy potential depending on stacking orders SP, AB (BA), and AA.[18] Adapted with permission from ref 18. Copyright 2013 Proceedings of the National Academy of Sciences. (c) Dark-field transmission electron microscopy images obtained by selecting the graphene diffraction peak (g = 1010) in TBG with various twisted angles. The alternating contrast of triangular domains is associated with the antisymmetric shift of the lattice period in AB and BA domains.[32] (d−f) Observation of atomic reconstruction in $MoSe_2$/WSe_2 heterostructures. (d) Diagram for the 0° + δ (R-type) and 60° + δ (H-type) heterostructure. The atomic registry for AB, BA, and ABBA stackings is labeled in green, yellow, and red circles and illustrated in the side view, respectively. (e) Stacking energy as a function of stacking orders along the red line labeled in (d). AB, BA, and ABBA structures are the global minima, which suggests that the structure will reconstruct to maximize the area of AB, BA, and ABBA domains. (f) Conductive AFM image of a 0.4° R-type and 0.6° H-type heterostructure showing alternating triangular domains of different conductivity and hexagonal domains with the same conductivity separated by domain boundaries of different conductivity, respectively.[31] Adapted from ref 31. Copyright 2020 American Chemical Society. (g) Illustration of the vdW assembly process to fabricate encapsulated twisted Gr/hBN device by hBN.[40] Adapted with permission from ref 40. Copyright 2019 AAAS. (h) Schematic of the PE-CVD method to prepare moiré pattern with graphene.[42] Adapted with permission from ref 42. Copyright 2020 Elsevier. (i) Structure of the graphene on nanosphere systems. Top panel: schematic showing graphene deposited on monolayer hcp-SiO_2 nanospheres (NS). Bottom panel: cross-sectional bright-field scanning transmission electron microscopy image of graphene on 20 nm NSs (blue dashed line).[36] Adapted from ref 36. Copyright 2018 American Chemical Society. (j) Illustration of the two individual moiré patterns and supermoiré patterns for three overlapping hexagonal lattices.[40] (k) (Top) Schematic illustration for the vector superposition of the second harmonic (SH) electric fields, where $\overrightarrow{E_1}(\omega)$ is the electric field of the fundamental light, $\vec{E}_1(2\omega)$ [$\overrightarrow{E_2}(2\omega)$] is the SH electric field from the flake 1 (flake 2), and $\vec{E}_S(2\omega)$ is the resulting SH electric field from the stacking region. (Bottom) Schematics for stacked bilayers with an arbitrary stacking angle θ, θ = 0°, and θ = 60° (or θ = 180°).[44] Adapted from ref 44. Copyright 2014 American Chemical Society. (l) Characterization of twisted angle by metallic line on the substrate and hemispherical handle.[43] Adapted with permission from ref 43. Copyright 2017 Proceedings of the National Academy of Sciences.

mentation of the periodic substrates.[36,37,39,52] The twisted angles of different moiré superlattices can be characterized by diverse optical ways.[40,42−44]

This emerging field of graphene research is expanded by the idea to stack a second layer of graphene on an existing graphene with a twisted angle, i.e., twisted bilayer graphene (TBG). By varying twisted angles, a moiré superlattice with different periods due to different stacking orders can form in the TBG, as shown in Figure 1a. There are energetically favorable AB and BA Bernal stacking orders and unfavorable AA stacking order (Figure 1b) connected by a saddle point (SP). SP has an energy of 2.1 meV/atom, 10 times lower than that of AA stacking.[18] Kim *et al.* found that the bilayer graphene with a small twisted angle (up to 0.8°) experienced atomic reconstruction (Figure 1c), leading to changes in lattice symmetry and electronic structure.[32] Similar to TBG, different stacking configurations also exist in TMDC bilayers. In $MoSe_2$/WSe_2 heterostructures, Rosenberger *et al.* observed two energetically degenerate commensurate configurations (AB and BA) in R-type stacking (0° + δ) but only one energetically favorable lattice arrangement (ABBA) for H-type stacking (60° + δ) (Figure 1d,e).[31] They also found alternating triangular domains with different conductivity and hexagonal domains with the same conductivity separated by domain boundaries of different conductivity in small-angle twisted R-type and H-type through conductive atomic force microscopy

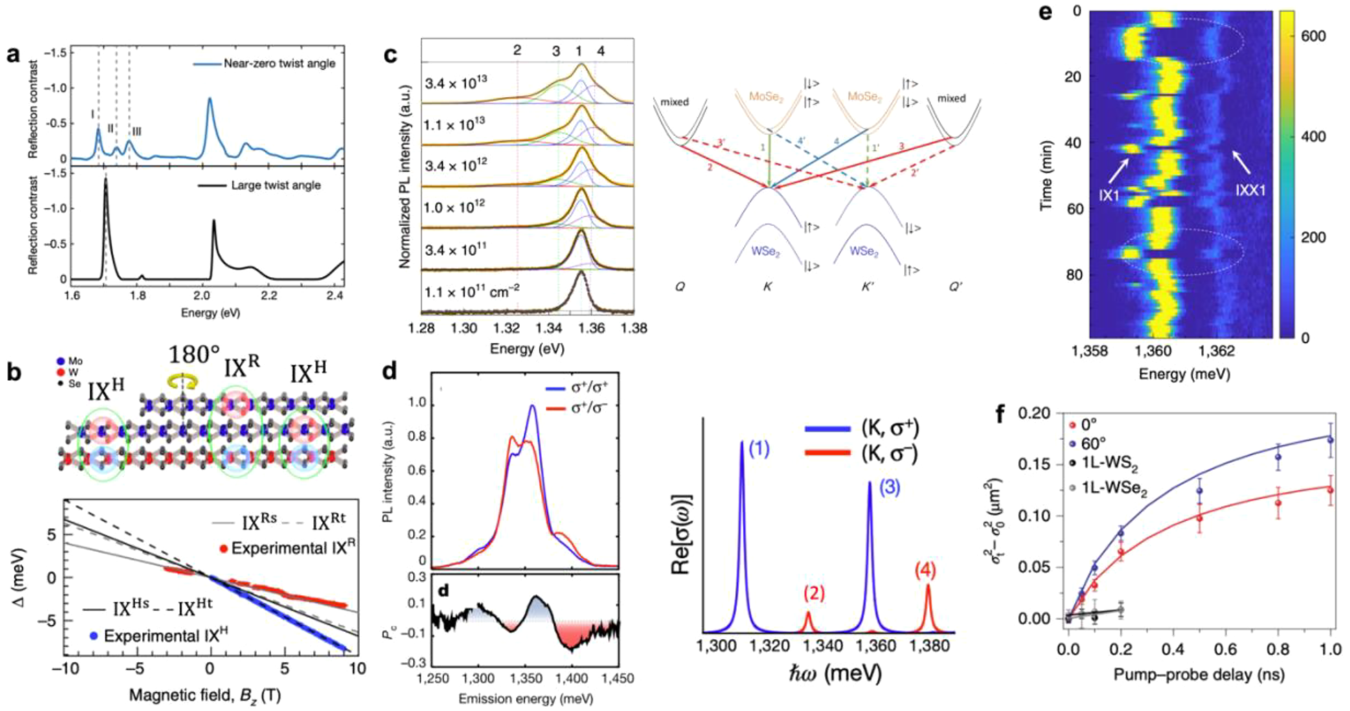

Figure 2. Signatures of moiré exciton in twisted 2D materials. (a) Reflection contrast spectrum of WS$_2$/WSe$_2$ heterostructure with near-zero twist angle (light blue, top) and a large twist angle (black, bottom).[47] Reprinted with permission from ref 47. Copyright 2019 Springer Nature. (b) Sketch of the trilayer heterostructure with bilayer MoSe$_2$ on top of monolayer WSe$_2$ (top).[61] The total valley-selective splitting of the interlayer transitions (Δ) for each IX species and spin-configuration as a function of the magnetic field (B$_z$).[61] IX^{Hs}, IX^{Rs}, IX^{Ht}, and IX^{Rt} represent excitons from spin-singlet (s) and spin-triplet (t) optical transitions with H- or R-type.[61] Reprinted with permission from ref 61. Copyright 2020 Springer Nature. (c) (Left panel) Excitation density-dependent PL spectrum of 1D moiré exciton.[62] (Right panel) Possible origin of each exciton shown in the left panel.[62] Reprinted with permission from ref 62. Copyright 2019 Springer Nature. (d) Circularly polarized photoluminescence (PL) spectrum performed at 15 K for σ^+ excitation from MoSe$_2$/WSe$_2$ heterobilayer with 1° twist angle (upper panel, left).[46] The degree of circular polarization as a function of the emission wavelength obtained from the PL spectra (lower panel, left).[46] Simulated optical conductivity of interlayer excitons in the K valley in response to σ^+ (blue line) and σ^- (red line) polarized light (right).[46] Reprinted with permission from ref 46. Copyright 2019 Springer Nature. (e) Time-resolved PL emission of localized interlayer excitons and biexcitons in MoSe$_2$/WSe$_2$ heterobilayer.[63] White arrows and dotted circles highlight the same spectral jittering patterns from IX1 (exciton 1) and IXX1 (excited state of exciton 1).[63] Reprinted with permission from ref 63. Copyright 2020 Springer Nature. (f) Diffusion width ($\sigma_t^2 - \sigma_0^2$) as a function of the pump−probe delay at 295 K for different twisted angles.[45] The blue and red lines are fits considering the repulsive interaction between the interlayer excitons.[45] The interlayer exciton transport in the heterobilayers is also compared with the exciton diffusion in 1L-WSe$_2$ and 1L-WS$_2$[45] along with the linear fits (black and gray lines). Reprinted with permission from ref 45. Copyright 2020 Springer Nature.

(CAFM) (Figure 1f), respectively. They attributed different domain shapes to the atomic reconstruction originated from a tendency of the system to stay in a lower overall energy state.

The essential process in the twisted field is to prepare and realize precise angle control between layers. The most popular way to prepare moiré patterns is called the vdW transfer technique.[40,51] This technique is based on the polymer transfer, mechanically exfoliating and stacking the thin materials using polymer stamp. Many researchers have realized some emerging properties in TBG devices[22,23] and twisted TMDCs with this vdW transfer method.[47,53,54] As shown in Figure 1g, graphene or a TMDC monolayer can be prepared by exfoliation or through CVD growth[55] first. Then the hBN is picked up from the prepared substrate at 70 °C by an adhesive polymer film (PPC)-coated polydimethylsiloxane (PDMS) stamp as a first layer and some part of graphene or TMDC successively lifted. After that, the remaining part of graphene or TMDC on the substrate is rotated at a controlled angle. Then the remaining part of graphene or the TMDC is picked up again with the PDMS stamp, constructing TBG or twisted TMDCs. This stack can be located onto another hBN layer to fabricate the encapsulated structure or on a thin SiN membrane for transmission electron microscopy (TEM) research. Recently, Zhu *et al.* developed an advanced mechanical way to achieve large-area and high-quality monolayer vdW materials using an atomically flat gold tape.[41]

In addition to mechanical exfoliation, CVD growth is an alternative way to prepare moiré patterns. Chen *et al.* succeeded to achieve millimeter-size twisted bilayer graphene with a plasma-enhanced CVD (PE-CVD) method (Figure 1h) on Cu foil directly.[42] The CVD growth method has been widely used to grow diverse 2D materials with large area which cannot be easily achieved by mechanical exfoliation.[56−59] In addition, they found the twisted angle was affected by the partial pressure ratio between the flowing reactant gases CH$_4$ and H$_2$. Another way to prepare a moiré superlattice is through transferring the 2D materials on the periodic substrates composed of nanospheres or micropatterns, as Zhang *et al.* reported (Figure 1i).[36,37,39,52]

Characterization of the twisted angles is as important. While many researchers measured the twisted angles using optical ways through the edge angle of each layer from microscopy images and SEM images (Figure 1j),[40] some groups used a more efficient way by depositing the metallic ruler on the substrate to measure the controlled twisted angle, as shown in Figure 1l.[43] However, sometimes the monolayer boundaries were not quite clear in the images, greatly increasing the uncertainty (~1°) in these two methods. In this case, more accurate optical measurement techniques were combined to investigate the twisted angles. The Raman spectroscopy,[42] which collected lots of data from many twisted samples with the information on relative intensity ratio of different signature modes as a function of twisted angles, was applied to decrease the uncertainty of the measured twisted angles assisted by the atomically resolved scanning tunneling microscopy (STM). In addition, the second harmonic generation (SHG) technique,[44,60] which decouples the coherent superposition of SHG signals from each monolayer, was widely used to determine the crystallographic orientation of materials. The SHG signal depends heavily on the polarization of the monolayer, and the decoupled SHG signals from the top and bottom layers can give the information on the stacking/twisted angle. Combining Raman spectroscopy and SHG techniques (Figure 1k), the uncertainty can be decreased (~0.01°),[44,49,55] essential for understanding the emerging properties discovered in the research.

MOIRÉ EXCITONS

The moiré excitons are the excitons trapped in the moiré potential minimum, given that their kinetic energy is less than the moiré potential.[47] They have different energy scales compared with the normal intralayer or interlayer excitons for 2D materials. Experimentally, individual layers with C_3 symmetry were usually chosen to study, such as $MoSe_2$ and WSe_2.[46,47,64] The moiré exciton would possess the same valley polarization as the local atomic registry and have a uniform g-factor across the sample.[64] This feature distinguishes moiré excitons from the defect-trapped excitons, where the potential distribution is usually randomized.[64] However, with high incident laser power, the traps created by the moiré potential can be filled up, and the emission will be broadened, similar to the defect-trapped excitons.[46,47,62,64] Therefore, in order to study the moiré exciton, the incident power should be low.[64]

As discussed above, the moiré exciton is trapped locally. Therefore, the first step is to know the location of the potential minimum spatially. There are usually two types of potential minimum points for TMD, which are called R-type or H-type.[48,61] Different alignment in the real space results in a different alignment of the valleys in the reciprocal space, changing the optical selection rules.[61,65] By combining multiple optical techniques,[65] the optical selection rules can be resolved for the moiré excitons. Thus, the physical property associated with each moiré exciton can be understood, such as spin-angular momentum. However, the location of the conduction band minimum after stacking remains elusive. For WSe_2 or $MoSe_2$, the valley is located in K or K′ point for individual layers. However, when they were stacked together, Gillen *et al.* suggested that the conduction band minimum move to another valley due to the hybridization.[62,66,67] This is important because the optical selection rule is associated with the specific valleys.

After creating the moiré exciton, the next step would naturally be either to manipulate it or to further understand the exciton−exciton interaction at a high carrier density. The latter one can be understood as creating an "advanced" moiré exciton state. This is interesting because it could provide a suitable platform to study the many-body physics, such as supersolids.[63,68,69] However, in several studies, more than one exciton showed up, with several or many sharp peaks even at seemingly low intensity.[46,47,61,62,64] The question now would be whether it is from the interplay of the original lattice potential and moiré potential, or it is affected by other factors, like the strain or defect, and, most importantly, whether this effect is linear or nonlinear. In other words, it is worth knowing both the intrinsic properties of the moiré exciton and how it would behave under external disturbance. In the following, we briefly survey some of the representative studies.

As one of the initial experiments, Jin *et al.* observed the three moiré excitons (labeled I, II, and III in Figure 2a, top) in the WS_2/WSe_2 heterostructure at 10 K.[47] At a twisted angle larger than 3°, these three peaks would completely disappear, with only the A exciton of WSe_2 left (peak around 1.7 eV, Figure 2a, bottom). The authors modeled the moiré potential as a periodic potential in addition to the original effective Hamiltonian and successfully reconstructed the transition from the single peak to three peaks by setting the moiré potential from 0 to 25 meV. From the simulation and experimental results, the moiré potential should be stronger at small angles (<1°) in this system. On the other hand, both gate-dependent reflection contrast spectrum and simulation suggested that these three moiré excitons were localized differently in the real space. Therefore, intrinsically, multiple moiré excitons can appear in the PL spectrum at low laser intensity but are associated with different spatial locations.

Experimentally, if we choose materials with a certain symmetry, how the angular quasi-momentum of moiré exciton is related to the original intra- or interlayer exciton is the key to understand the moiré potential. In addition to the observation of intralayer moiré excitons in WS_2/WSe_2 heterobilayer,[47] Jin *et al.* identified the higher-energy interlayer moiré excitons with helicity-resolved photoluminescence excitation (PLE).[65] With resonant pump−probe spectroscopy, the authors skillfully inferred different quasi-angular momentum by comparing the circular dichroic signal of the moiré interlayer excitons to the known intralayer exciton. In particular, the moiré quasi-angular momentum was determined for different interlayer moiré exciton states. Later on, with an uncommon trilayer sample geometry, Brotons-Gisbert *et al.* observed a distinct interlayer moiré exciton species (R-type) at lower energy (~1.26 eV) by stacking a bilayer 2H-$MoSe_2$ on top of a monolayer WSe_2 (Figure 2b, top).[61] Due to the 180° rotation between the top and bottom $MoSe_2$ layer, the spin and valley configuration was reversed in the upper layer. This was confirmed by the magneto-optical spectroscopy measurement (Figure 2b, bottom), where the effective g-factors were distinct for these two exciton regions across the sample, leading to different energy splitting for R-type (between the upper layer of $MoSe_2$ and WSe_2) and H-type (between the bottom layer of $MoSe_2$ and WSe_2) configurations. In addition, the experimental results (red and blue dot) for energy splitting under an external magnetic field agreed well with the calculation based on the assumption of the spin-valley configuration in each layer, indicating that the spin and valley were still locked in this three-layer system. Further study needs to be done to determine the maximum number of layers to preserve this locking effect.

In the following, we want to discuss three different disturbance sources (domain reconstruction, band hybrid-

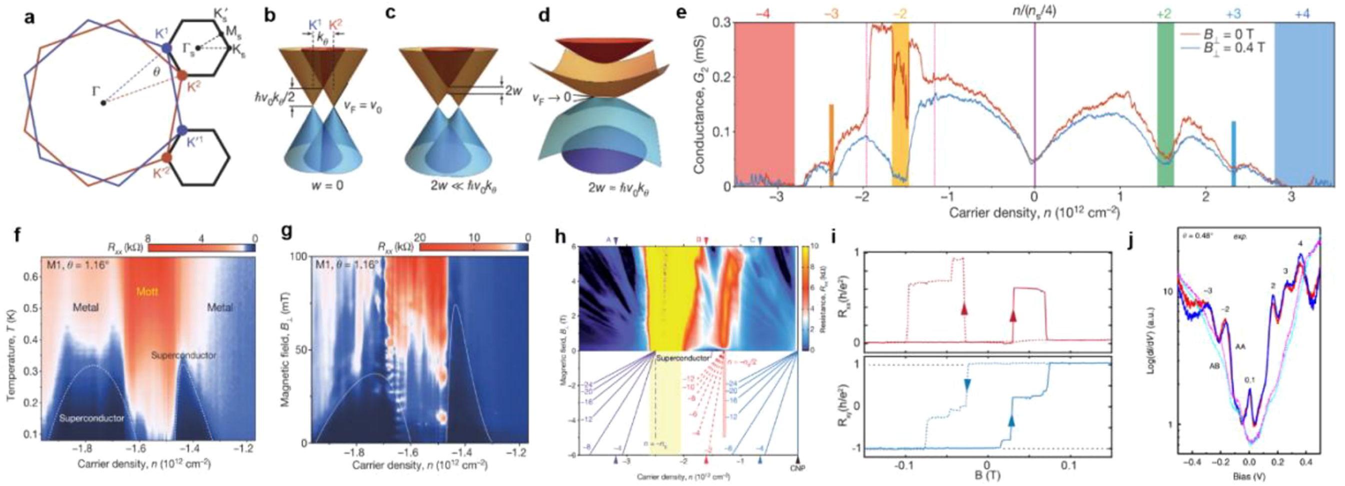

Figure 3. Correlated insulating states and superconductivity. (a) Mini-Brillouin zone arises from displacement of K wavevectors in two layers of tBLG.[22] (b−d) Illustration of the effect of interlayer hybridization for hybridization energy $2w = 0$ (b), $2w \ll \hbar v_0 k_\theta$ (c), and $2w \approx \hbar v_0 k_\theta$ (d) in tBLG, where $2w$ is hybridization energy and $\hbar v_0 k_\theta$ is kinetic energy.[22] Adapted with permission from ref 22. Copyright 2018 Springer Nature. (e) Existence of correlated insulating states at integer fillings, accompanied by the superconductivity, measured at $T = 70$ mK, $V_{\text{bias}} = 10\ \mu$V.[23] (f,g) Phase diagram of magic angle tBLG, including temperature-dependent (f) and magic-field-dependent at $T = 70$ mK (g).[23] (h) Quantum oscillation pattern in tBLG.[23] Adapted with permission from ref 23. Copyright 2018 Springer Nature. (i) Hysteresis loop and quantized anomalous Hall effect with $C = 1$ at $B = 0$, 3/4 filling in tBLG.[71] Adapted with permission from ref 71. Copyright 2020 AAAS. (j) Appearance of pseudo-Landau level in AA stacking region in tBLG at $\theta = 0.48°$.[72] Adapted with permission from ref 72. Copyright 2020 Springer Nature.

ization, and strain), which might modify the behaviors of the moiré exciton.

A recent study done by Sung *et al.* gave insights into the impact of the crystal symmetry of reconstructed domains on excitonic properties in twisted $MoSe_2$ homobilayers.[70] They claimed that the different sign of Stark slope and avoided crossing indicated the opposite dipole orientation of excitons in AB and BA stacking.[70] The authors confirmed that the distribution of electrons was not in mirror symmetry at the top and bottom layer for AB stacking with density functional theory (DFT) calculations. So, the dipole orientation of excitons is actually flipped in BA stacking, which is why the sign changes.

Hsu *et al.* studied the interlayer valence band hybridization (hybridized holes) for heterobilayers ($WSe_2/MoSe_2$, WS_2/MoS_2) and a homobilayer (MoS_2/MoS_2) with different stacking configurations at the K point.[48] With hybridization, a "mixed" state of inter- and intraexciton, possessing both large optical and electric dipole moment, is realized. The authors demonstrated that the interlayer hopping integral determines whether it is possible to have the hybridization happen, leading to band splitting.

As shown in Figure 2c, Bai *et al.* systematically investigated the impact of the strain on the moiré potentials by piezoresponse force microscopy (PFM).[62] Apart from the 0D typical moiré landscape, a stripe-like 1D moiré landscape was observed under the uniaxial strain. Although the PL peak shapes of 0D and 1D are different at low excitation, the peak widths of both 0D and 1D moiré excitons were broadened with increasing incident power. At high excitation density, the PL shape of 0D and 1D moiré excitons showed similar features, and both of them could be deconvoluted by four PL peaks, suggesting that they may have the same origin. One possible reason could be that three of the peaks originate from the excitons outside the moiré traps.

In addition to the study that focused on the noninteracting condition for moiré excitons, whether the moiré potential can have considerable effect on exciton−exciton interactions remains largely unexplored. Several different and plausible explanations were proposed, yet it remains, for example, unclear the impact of nonlinearity on moiré potential.

With the same heterobilayer structure, Tran *et al.* also observed four excitons. They studied the polarization of different excitons and gave insights into the possible origins. The four excitons showed alternating circular polarization, defined as $P_c = \frac{I_{co} - I_{cross}}{I_{co} + I_{cross}}$ (Figure 2d, left).[46] Unlike Bai's explanation, different emissions were simulated and attributed to the ground- and excited-state interlayer excitons within one moiré potential well (Figure 2d, right). On the other hand, the strong interaction of moiré excitons was indirectly suggested by several experiments.[45,63] As Li *et al.* reported with $MoSe_2/WSe_2$, multiple excitons could be trapped in a single localized quantum well with strong nonlinear behaviors at very low incident laser intensity (~μW).[63] From the time-resolved PL measurement, the synchronized spectral jittering (Figure 2e) of two close narrow interlayer exciton peaks indicated that they were trapped in the same local quantum well. The peak with larger photon energy is likely to be a biexciton based on the power-dependent measurement results. However, whether the observed localized interlayer excitons originate from moiré potential (twist angle 2−6°) or defects still lacks solid proof, since the PL spectrum lacked strong valley polarization. Nevertheless, the authors attributed the lack of valley polarization to the local strain, which reduced the symmetry of the moiré pattern. Meanwhile, Yuan *et al.* studied the influence of moiré potential to the interlayer exciton migration in CVD grown WS_2/WSe_2 heterobilayer.[45] Similar to Li, the authors found that the exciton−exciton interaction was strong, and the diffusion could not be simply modeled by a constant diffusion coefficient. Figure 2f shows the time-dependent

https://doi.org/10.1021/acsnano.0c10435
ACS Nano XXXX, XXX, XXX−XXX

exciton diffusion length for 0 and 60° heterobilayers, monolayer WS_2 and monolayer WSe_2, respectively. The diffusion length is much longer in the heterobilayer, where the trend was nonlinear. By including the interaction between the excitons, the nonlinear feature can be resolved. Moreover, the largely increased exciton diffusion velocity compared to monolayer cases could also be explained by the strong repulsive force among the excitons. At the same time, the authors simulated the moiré potential for 0 and 60° heterobilayers. The higher moiré potential at 0° explains the smaller diffusion velocity at 0°.

In summary, the moiré potential created by stacking the 2D materials is unordinary in the sense of the energy and spatial scale. Therefore, the interaction between the moiré potential and the original lattice potential is very different compared with other external potentials. Thus, the total potential might be nontrivial, and the quasi-angular momentum would be affected. Also, some external disturbances, such as the domain reconstruction, band hybridization, and strain, would modify the behaviors of the moiré exciton. On the other hand, since some indirect proof was given for the strong interaction of the moiré excitons, how to further calibrate it should be an ongoing project.

SUPERCONDUCTIVITY AND FERROMAGNETISM

In addition to the exceptional moiré exciton features brought by the moiré pattern, it also supports the study of correlated states including the Mott insulating state as well as unconventional superconductivity.[73] A more detailed and in-depth review for this part can be found elsewhere.[20,74,75]

Moiré lattice is formed when two monolayer graphene are stacked with a slight angular displacement, leading to the emergence of a mini-Brillouin zone in reciprocal space (Figure 3a). At a small twisted angle, two adjacent Dirac cones at K (or K′), contributed from the upper and lower layer, respectively, were mixed through hybridization due to interlayer hopping.[76,77] The hybridization opened up a band gap near the intersection of adjacent cones and reduced Fermi velocity at the Dirac cones,[78−81] indicating the formation of flattened bands near the charge neutral point (CNP) (Figure 3b−d). At a series of magic angles, where zero Fermi energy at Dirac points appears, the width of flattened band could be less than 10 meV, separated from other bands by single-particle gaps.[22,23,76] Calculation showed that the first magic angle was about 1.1°,[76] around which most of the research has been conducted. The alignment of hBN (capsule) can be used to break C_2 symmetry, thus opening up the band gap in the Dirac point, causing insulating behavior at the CNP.[82] Correlated insulating states showed up at integer fillings when Coulomb interaction energy U between electrons was larger than the kinetic energy, around which superconductivity was observed experimentally, as discussed in detail later. Note that given the four-fold degeneracies for the spin and valley, the integral filling represents carrier density $n = \pm\frac{n_s}{4}, \pm\frac{n_s}{2}, \pm\frac{3n_s}{4}$, corresponding to 1/4 filling, 1/2 filling, and 3/4 filling, where n_s is when the lowest energy superlattice bands are fulfilled. When $n = n_s$, the system shows an insulating state due to the band gap opened by hybridization.[78]

Since the observation of unconventional superconductivity in tBLG near magic angle by Cao *et al.*,[22,23] various related work has flourished. Experimentally, the sample was usually encapsulated by hBN, with Hall bars deposited to probe transport properties. Carrier density was controlled by a back-gate or dual-gate structure, and the latter one could also generate a displacement field to tune correlated insulating states.[21] Based on this gate tunability, a phase diagram within a wide range of charge densities was probed, showing the existence of correlated insulating states and superconducting states at and around certain integer fillings (Figure 3e−g).[21,23,49]

The correlated insulating states with conductivity maxima were observed at integer fillings within flat bands. The main evidence for the existence of 2D superconductors was the zero resistance at low temperature and small magnetic field and the dependence of the critical current as a function of temperature and magnetic field.[20,21,49,83] The quantum interference pattern where critical current oscillates with magnetic field also indicates the presence of percolating superconductivity. The observation of the coexistence of superconducting and correlated insulating states gives rise to the possibility that two states share the same origin, and also that the superconductivity can be unconventional, as the phase diagram is similar to that of cuprate superconductors, driven by electron−electron interaction.[22,23,83−90] However, recent studies showed superconducting states without the coexistence of a correlated insulating state,[91,92] providing critical evidence for electron−phonon coupling driven superconductivity, as supported by theoretical models, as well.[93−95]

As shown in Figure 3h, quantum oscillation is presented as magnetoresistance (R_{xx}), changing with carrier density within flat bands. The oscillation pattern provides detailed band structure information.[21] Away from the magic angle, resistance minimum forms sets of Landau fans that originate from the CNP, indicating the eight-fold degeneracy at the CNP that can be understood as doubled four-fold spin-valley degeneracy in monolayer graphene.[78] However, near the magic angle, degeneracy at the CNP always reduces to four-fold. Also, additional sets of the Landau fan with lower degeneracy originate at integer fillings where correlated insulating states exist, suggesting the formation of different Fermi surfaces. Two-fold degeneracy was usually observed at $n = \pm\frac{n_s}{2}$, and the mechanism of the lifted degeneracy is still under debate.

However, the critical temperature, carrier density where correlated states occur, and degeneracy can be greatly affected by device properties such as twisted angle inhomogeneity. When the twisted angle was close to the magic angle, the single-particle bands were flatter and higher T_c was detected.[20] Inhomogeneity, caused by nonuniform strain,[96−101] rotation angle,[21,32,102,103] and charge distribution,[104] can be mapped by STM,[79,81,96,97,100,105,106] TEM,[18,29,32,107] and SQUID-on-tip.[108,109] Lu *et al.* observed insulating states at all integer fillings and more superconducting domes at lower carrier densities with lower inhomogeneity.[49] It is worth mentioning that there are parameters that can be used to tune the correlated states, including pressure and displacement field.[21]

Additionally, other peculiar transport properties were also observed. Careful alignment of hBN onto tBLG at the magic angle breaks the C_2 rotation symmetry of tBLG, causing nonzero and opposite Chern numbers for flat bands in each valley, which, combined with spontaneous valley polarization,[82,110] gives rise to quantum anomalous Hall effect at $n = \frac{3n_s}{4}$ with $C = 1$[50,71] (Figure 3i) and $n = -\frac{n_s}{2}$ with $C = 2$.[91] Pseudomagnetic field (PMF) is formed through the nonuniform strain of graphene, where strain distorts the K and K'

valleys in the graphene Brillouin zone without breaking the sublattice symmetry, showing a similar effect on carriers by a perpendicular external magnetic field.[111] Since structure deformation can be introduced by a moiré pattern, PMF has already been experimentally realized in low-angle tBLG with a rotation angle less than 1°,[72] and in a graphene−black phosphorus heterostructure,[112] a pseudo-Landau level is detected in both of those structures (Figure 3j). The existence of PMF provides another way to achieve the quantum anomalous Hall effect as well as the quantum valley effect. Unconventional ferroelectricity is recently realized in the bilayer graphene/boron nitride moiré system, originated from charge transfer between layer-polarized moiré flat bands under a displacement field.[113] In addition, small-angle twisted boron nitride shows spontaneous formation of a ferroelectricity-like domain where high density of the interfacial dipole is observed.[114] Similar phenomena are expected to be explored in other similar twisted 2D structures, indicating rich physics in the moiré structure. Correlated states were also observed in other 2D heterostructures at their magic angles, such as ABC-trilayer graphene/hBN,[115−119] twisted double bilayer graphene,[120−124] and TMDCs.[125−128] ABC-trilayer graphene/hBN showed gate-tunable Mott insulating states at 1/2 filling and 1/4 filling and gate-tunable superconductivity at 1/4 filling on both hole- and electron-doping sides.[117−119] Also, correlated Chern insulator with $C = 2$ and ferromagnetism were observed at 1/4 filling at the hole-doping side when applying a vertical displacement field.[115−117] In twisted double bilayer graphene, correlated insulating states at integer filling can be largely affected by an in-plane magnetic field, indicating the existence of spin-polarized ground states.[120,121,123,124] The superconductivity at half-filling was also enhanced by an in-plane magnetic field, suggesting the dominance of the spin-polarized electron paring mechanism.[121] Twisted bilayer WSe_2 held a larger magic angle, around which correlated states existed within a wider range.[127,128] In WSe_2/WS_2, correlated states were also observed at 1/3 and 2/3 fractional filling of a hole-side flat band, due to the generalized Wigner crystallization.[126] In addition, antiferromagnetic Curie−Weiss behavior appeared at half-filling of first hole band, transiting toward the ferromagnetic state by hole-doping.[125] Moreover, the insulating state at half-filling of hole-side flat bands was observed in both twisted bilayer WSe_2 and WSe_2/WS_2, with superconductivity existing around half-filling in twisted bilayer WSe_2.[125,126,128]

Overall, various research studies have been conducted; however, the variations within results lead to the difficulty in explaining the phenomena. Furthermore, the explorations on twisted materials beyond tBLG are still in the early stages. There is still a long way to go before developing a systematic theory on twistronics.

RECONSTRUCTED MOIRÉ PATTERNS AND SOLITONS/DOMAIN WALLS

The previous sections addressed the emergent properties observed and explained in the vdW materials under the rigid lattice assumption; however, the interplay between the vdW force and the elastic energy at the interface can cause atomic reconstruction.[32] Recently, there has been increasing research interest in the nature of atomic reconstruction at small angles. Figure 4 lists the atomic reconstruction regions reported so far with a small angle range in bilayer graphene (<1.1°) and a relatively large angle range in bilayer TMDC (<5°), where the lattices were strained locally to maximize the size of the energetically favorable AB/BA stackings. In this section, we focus on the effects from the rearrangement of the atoms within the individual layers.

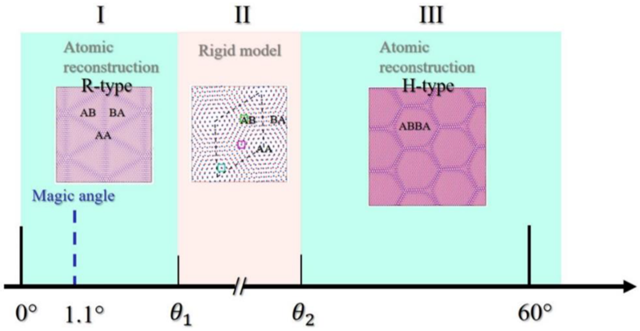

Figure 4. Atomic reconstruction region schematic. Experimental discovery of the atomic reconstruction regions in small angles near the symmetry stackings in the vdW materials. The "magic angle" is defined in the graphene where unconventional superconductivity appears. The values of θ_1 (∼5°) and θ_2 (∼51°) are dependent on the materials. Insets are reprinted with permission from ref 38. Copyright 2018 American Physical Society.

Recent theoretical work on graphene/graphene[38,129] and twisted TMDC structures[33,38,130] and experimental work on bilayer graphene,[18,29,107] bilayer hBN,[24] graphene/hBN,[34] bilayer TMDC,[30] and $MoSe_2/WSe_2$ heterostructures[31] indicate that the atomic reconstruction can occur under translational shifts or at small twisted angles and solitons/domain walls can form. The behavior of the domain walls is complex, consistent with the complex atomic arrangements at the domain walls.[25,31,32,38]

In the bilayer graphene, graphene/hBN and bilayer hBN, atomic reconstruction has been found to be significant when the twisted angle $\theta \lesssim 1°$[32,34] *via* CAFM,[34] transmission electron microscopy (TEM),[18,32,107,131] and STM.[34] The structural,[29,34,107] mechanical,[18,24] and electronic properties[25,70] of the domains and domain walls have been demonstrated. Lin *et al.* reported the existence of nanometer-wide strained channels, most likely in the form of ripples, between Bernal stacked bilayer graphene regions with translational shift.[29] Ni *et al.* found that the domain wall width varied with moiré period in monolayer graphene/hBN (Figure 5a).[34] Larger period (*i.e.*, smaller twisted angle) will lead to narrower domain walls. In addition, the relative lattice constant in the domain wall region is smaller than that in the uniform areas (Figure 5b).[34] This is a strong proof of lattice reconstruction.

To reveal the structural and mechanical property of the domain walls, dark-field TEM was used to observe soliton motion in the bilayer graphene under translational shift,[18] and strain field was analyzed.[24,107] Alden *et al.* found that, under the influence of the beam, soliton boundaries undergo topological rearrangement with position fluctuation and solitons with opposite directions can annihilate after contacting (Figure 5c).[18] In addition, with implemented Burgers vector analysis, Butz *et al.* developed the strain distribution associated with deformed lattices and revealed the origin of the solitons.[24,107] Meanwhile, the electronic property can also be significantly changed. Huang *et al.* demonstrated the emergence of topologically protected helical (TPH) states on the domain walls at the energies where AB and BA (like Figure

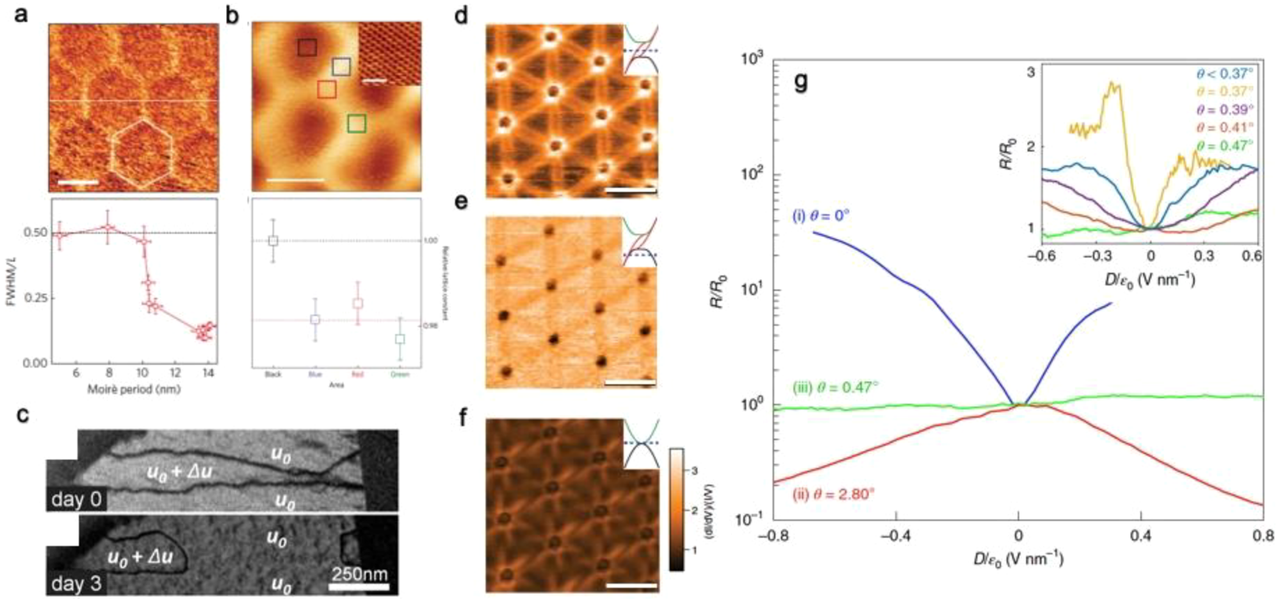

Figure 5. Reconstructed moiré pattern and solitons in vdW materials. (a) Young's modulus distribution in graphene/hBN sample, measured by conductive AFM in the PeakForce mode, for structures with 14 nm moiré patterns. The scale bar is 10 nm. The bottom figure shows the ratio between fwhm of the peak in the Young's modulus distribution and the period of the moiré structure *L*, as a function of the period of the moiré structure for several samples.[34] (b) STM image of fully aligned monolayer graphene on hBN. Both the moiré pattern and the atomic structure are resolved. The scale bar is 10 nm. Inset shows a zoned-in figure of the region marked by black square with scale bar of 1 nm. The bottom figure shows the relative lattice constants for different areas within moiré patterns shown in the top figure marked with different colors correspondingly.[34] Adapted with permission from ref 34. Copyright 2014 Springer Nature. (c) Dark-field TEM images show soliton motion with two solitons having opposite translation directions, Δ*u*, seeming to have contacted each other and annihilated.[18] Adapted with permission from ref 18. Copyright 2013 Proceedings of the National Academy of Sciences. Density of states mapping by STM with (d) sample voltage −0.11 V and back-gate voltage +60 V, (e) sample voltage −0.245 V and back-gate voltage +60 V, and (f) sample voltage 0.1 V and back-gate voltage −50 V. The scale bar is 50 nm, and the tunnel current is 200 pA (ac voltage is 8 mV). (Insets) Schematics of the band structure, with the sample voltage being probed marked by the blue dashed line. The green and black curves denote the conduction and valence bands of the Bernal stacked bilayer regions, respectively, whereas the red lines are due to the TPH states on the domain wall.[25] Adapted with permission from ref 25. Copyright 2018 American Physical Society. (g) Normalized Dirac peak resistances as a function of transverse displacement field. The inset shows a linear-scale plot of normalized Dirac peak resistances as a function of the electric displacement field, *D*, for small-angle TBG devices.[32] Adapted with permission from ref 32. Copyright 2019 Springer Nature.

1b) regions are gapped in the small-angle twisted bilayer graphene with a triangular moiré pattern through scanning tunneling spectroscopy (STS) (Figure 5d−f).[25] Furthermore, Yoo *et al.* observed the appearance of the secondary Dirac bands with the breakdown of a simple moiré band description and with increasing transverse electric displacement field *D*, the normalized longitudinal resistance (by the resistance at the global CNP) shows an increase and then saturated trend (Figure 5g) in small-angle ($\theta < 1°$) twisted bilayer graphene.[32] These electron transport behaviors are distinctly different from the Bernal stacked BLG ($\theta = 0°$) and the large-angle ($\theta > 1°$) TBG, where the resistance increases and decreases rapidly with increasing $|D|$, respectively. When $\theta = 0°$, the gap opens at the CNP due to broken inversion symmetry by large $|D|$, leading to larger resistance, and when $\theta > 1°$, the resistance decreases with increasing $|D|$ due to the weak interlayer coupling, and thus by increasing $|D|$, each layer will be doped with an equal amount but opposite sign of carriers, making both layers less resistive. This observation is consistent with the formation of a 1D network of conducting channels when AB/BA domains are gapped at high $|D|$.[25]

In addition to the atomic reconstruction findings in graphitic materials, increasing research interest has been spread into the TMDCs. Atomic reconstruction was reported to happen in homobilayer TMDCs with twisted angle $\theta < 3°$[30,33,70] and heterostructures with twisted angle $\theta \lesssim 3°$[33,132] *via* DFT calculations,[38,133] CAFM,[30,33] atomic-resolution scanning tunneling electron microscopy (STEM),[30] low-frequency Raman spectroscopy,[132] secondary electron microscopy,[134] and IR nanoimaging method.[135]

The vdW heterostructures give us the opportunities to achieve complex functionalities which do not exist in nature due to the precise stacking technique. Compared with twisted graphene, twisted homo- and heterobilayers provide a broader diversity of physical properties caused by lack of inversion symmetry. Most of the work related to the reconstructed moiré pattern has been done in twisted bilayer graphene; however, rare research reported the reconstruction in homobilayer TMDs, not to mention in the twisted bilayer heterostructures. The domain formation in 2D heterostructures was previously predicted.[38] Naik *et al.* predicted that the relative energy correlated strongly with the interlayer spacing, and the variance of the interlayer spacing increased as the twisted angle θ approaching 0 or 60° in the twisted bilayer MoS_2 (Figure 6a,b) through DFT calculations.[33] With simulation, Maity *et al.* predicted when $\theta \gtrsim 58.4°$ in the twisted homobilayer TMDs, the constant of the moiré lattices is $\sqrt{3}$ times that of the unrelaxed ones, and the width of domain walls is about 1 nm larger when θ approaches 60° than when θ approaches 0°.[133] Following the theoretical predictions, several experimental studies aimed to validate the atomic reconstructions in TMDCs. Rosenberger *et al.* measured CAFM for both R-

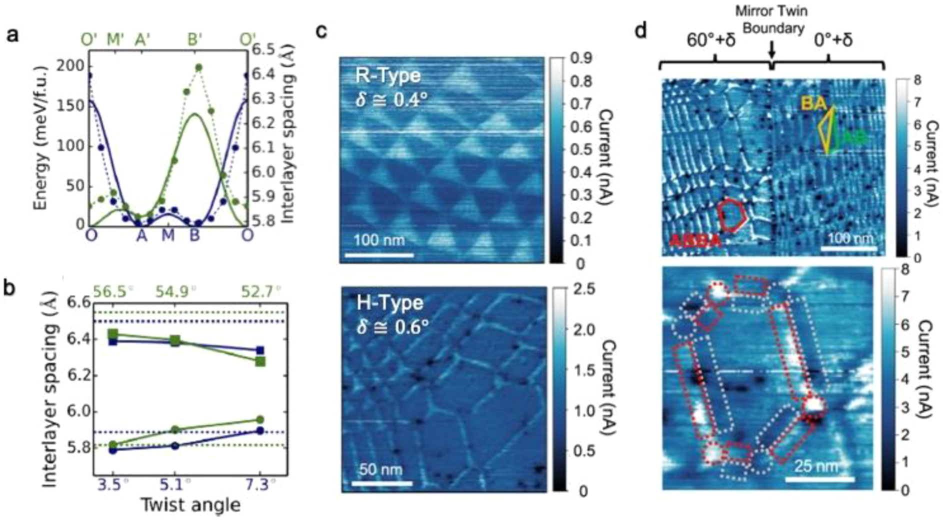

Figure 6. Reconstruction of moiré lattices in bilayer TMDC materials. (a,b) DFT calculations of the relative energy (a)[33] and interlayer spacing (ILS) (b)[33] of the stackings along a line traversing high symmetry stackings in the twisted bilayer MoS_2. The blue (green) lines correspond to the path in 3.5° (36.5°) angles. The solid (dashed) lines represent relative total energy (ILS) along the path. Maximum (squares) and minimum (circles) ILS as a function of twist angle are shown in the bottom figure. Adapted with permission from ref 33. Copyright 2018 American Physical Society. (c) CAFM images of a $MoSe_2/WSe_2$ heterostructure for R-type with $\delta = 0.4°$ and H-type with $\delta = 0.6°$ show triangular alternating domains of different conductivity and hexagonal domains separated by domain walls with different conductivity, respectively.[31] (d) CAFM images of a $MoSe_2/WSe_2$ heterostructure on graphite with sample bias $V_s = +0.8$ V. This sample has both R-type and H-type separated by a mirror twin boundary. The bottom figure shows a zoned-in image of CAFM for H-type. The hexagonal direction shows low conductivity (gray box) and high conductivity (red box) at domain walls. Also, the hexagon vertices alternate between low conductivity (gray circles) and high conductivity (red circles).[31] Adapted from ref 31. Copyright 2020 American Chemical Society.

type and H-type at small twisted angles (Figure 6c) in $WSe_2/MoSe_2$ heterostructures, showing alternating triangular domains (AB/BA) of different conductivity in R-type and hexagonal domains (ABBA) with the same conductivity separated by domain walls in H-type.[31] This observation agrees well with Figure 1d and cannot be explained by the rigid-lattice moiré pattern shown in Figure 1a. The size of the domains was found to vary with twisted angles, in the range of tens to 100 nm.[31] In addition, to further study the behavior of domain walls, CAFM images (Figure 6d) were taken on a $WSe_2/MoSe_2$ heterostructure on a graphite sample with a bias, showing both R-type and H-type domains separated by a mirror twin boundary. The enlarged CAFM image in Figure 6d for the H-type domain suggested complex domain behavior, which was consistent with the complex atomic arrangements at the domain walls predicted by the theory.[38] Further reinforcing this conclusion, Holler *et al.* explored interlayer shear modes (ISMs) with a twisted angle no larger than 3° in both R-type and H-type $WSe_2/MoSe_2$ heterobilayers using low-frequency Raman spectroscopy,[132] where the ISMs were only found in homobilayers due to the existence of restoring force in the commensurate configuration.[136−138]

Regarding the atomic reconstruction modification on the electronic structure of vdW heterobilayers, Weston *et al.* observed strong piezoelectric textures in the twisted 2H MoS_2/WS_2 bilayers and layer-polarized conduction band states in the twisted 3R bilayers.[30] The lack of both inversion and mirror symmetry in 3R stacking formed by lattice reconstruction allows the electron density wave function to be different on the same atom in the top and bottom layers, leading to different layer polarizations.[30] While in the 2H stacking, although the inversion symmetry appears, the opposite sign of the strain tensors due to the lattice reconstruction leads to the same sign for the induced charges, introducing high-density piezoelectric charge at the domain walls, especially at their intersections.[30] What's more, Enaldiev *et al.* claimed that the inhomogeneous strain brought by lattice reconstruction leads to the formation of spots of piezocharges where the domain walls cross with a combination of DFT and elasticity theory.[139] This makes the domain wall intersection sites attractive for optoelectronic studies.

In addition to these well-established methods, *in situ* atomic reconstruction has been directly observed experimentally by versatile nondestructive approaches, including secondary electron microscopy[134,140] and an IR nanoimaging method.[135] Sushko *et al.* demonstrated a SEM-based method, which uses a secondary electron microscope to directly image the local stacking order in fully hBN-encapsulated gated vdW heterostructure devices on standard Si substrates.[134] Luo *et al.* implemented the infrared-light into the nanoimaging method to realize direct observation of phonon polariton dynamics at the domain walls.[135]

Moreover, it is noteworthy that the atomic reconstruction has also been observed through combing hydrostatic pressure[141] with controlled rotational angles or mechanical strain, suggesting the tunability of optoelectronic properties in vdW heterostructures.[142] Yankowitz *et al.* found reasonable corrugations and strains in BN-encapsulated graphene by tuning the interlayer coupling strength with hydrostatic pressure along with the appearance of a secondary Dirac point which shows little dependence on pressure.[141] Lebedeva *et al.* predicted the formation of equilateral triangular network of domain walls with biaxial elongation of the bottom layer in bilayer graphene on the basis of the two-chain Frenkel−Kontorova model.[142]

OUTLOOK

Despite the rapid development in the study of moiré patterns in twisted vdW materials, there still remain many outstanding questions to be explored. Sung *et al.* observed opposite electric dipole moments at AB/BA regions in the near-0°-twisted bilayer $MoSe_2$, paving the path to achieve dipole moments "flipping", in addition to the external electric field.[70] In addition to that, Hu *et al.* unveiled photonic dispersion engineering in large-angle twisted evanescently coupled hyperbolic metasurfaces theoretically.[27]

While most of the research studies were focused on correlated electronic properties, a complete picture of the underlying mechanism for band structure evolution induced by atomic reconstruction remains elusive. First, mechanisms explaining the emerging properties, including unconventional superconductivity, do not fully account for the existence of atomic reconstruction. Second, the understanding of the spatial distribution of individual exciton and its dynamics has been limited by the spatial and energy resolution of the detection technique.

Furthermore, other carriers can also be affected by the moiré pattern, leaving a largely unexplored field. With the development of sample preparation methods and detection techniques, more and more emerging dynamics can be discovered, such as spin and valley dynamics and chiral phonon dynamics. Manipulation of spin and valley dynamics can give rise to the potential of overcoming the fundamental limits of speed and energy consumption by considering spin and valley as the information carrier. Wang *et al.* found long spin and valley lifetime in TMDC heterostructures through studies of spatiotemporal dynamics of spin and valley depolarization mechanisms.[143] A recent theoretical prediction showed the exciton g-factor in the van der Waals heterostructures was strongly spin- and stacking-dependent.[130] However, it remains unclear the possible effects of the moiré pattern on spin and valley dynamics and how it will affect the optical selection rules. This probably provides more degrees of freedom to manipulate the rate and efficiency of carrier transfer process.

AUTHOR INFORMATION

Corresponding Authors

Feng He — *State Key Laboratory on Tunable Laser Technology, School of Electronic and Information Engineering, Harbin Institute of Technology, Shenzhen 518055, China; Walker Department of Mechanical Engineering and Texas Materials Institute, The University of Texas at Austin, Austin, Texas 78712, United States;* Email: hefeng2020@hit.edu.cn

Yaguo Wang — *Walker Department of Mechanical Engineering and Texas Materials Institute, The University of Texas at Austin, Austin, Texas 78712, United States;* orcid.org/0000-0002-0448-5645; Email: yaguo.wang@austin.utexas.edu

Authors

Yongjian Zhou — *Walker Department of Mechanical Engineering, The University of Texas at Austin, Austin, Texas 78712, United States*

Zefang Ye — *Walker Department of Mechanical Engineering, The University of Texas at Austin, Austin, Texas 78712, United States*

Sang-Hyeok Cho — *Walker Department of Mechanical Engineering, The University of Texas at Austin, Austin, Texas 78712, United States*

Jihoon Jeong — *Walker Department of Mechanical Engineering, The University of Texas at Austin, Austin, Texas 78712, United States*

Xianghai Meng — *Walker Department of Mechanical Engineering, The University of Texas at Austin, Austin, Texas 78712, United States*

Complete contact information is available at: https://pubs.acs.org/10.1021/acsnano.0c10435

Author Contributions

$^\perp$F.H. and Y.Z. contributed equally.

Notes

The authors declare no competing financial interest.

ACKNOWLEDGMENTS

The authors are grateful for the supports from the National Science Foundation (NASCENT, Grant No. EEC-1160494; CAREER, Grant No. CBET-1351881, CBET-1707080, Center for Dynamics and Control of Materials DMR-1720595) and Harbin Institute of Technology (Shenzhen) startup funding.

VOCABULARY

Circular dichroic signal, the signal which reflects the difference in absorption of left- and right-handed circularly polarized light[144]; **unconventional superconductivity**, where Cooper pairs are not bound to exchange other than phonon exchange: the latter one refers to conventional superconductivity[73]; **correlated insulating state**, electron hopping is suppressed due to the much stronger Coulomb interaction between electrons within same orbital than the bandwidth, preventing electron transport through material[145]; **quantum anomalous Hall effect**, quantized Hall effect without external magnetic field: can be realized in system which can usually be achieved in ferromagnetic insulators with a strong exchange coupling[146]; **ferromagnetism**, a collective phenomenon since individual atomic dipole moments interact to align parallel to one another[147]; **ferroelectricity**, spontaneous electric polarization that can be reversed by external electric field, accompanied by hysteresis; **soliton**, a wave that preserves the shape and velocity after interaction; Frank and van der Merwe (1949) showed that incommensurability is tightly associated with the appearance of topological defects: solitons or domain walls

REFERENCES

(1) Huberman, S.; Duncan, R. A.; Chen, K.; Song, B.; Chiloyan, V.; Ding, Z.; Maznev, A. A.; Chen, G.; Nelson, K. A. Observation of Second Sound in Graphite at Temperatures Above 100 K. *Science* **2019**, *364* (6438), 375−379.

(2) Jin, C.; Kim, J.; Utama, M. I. B.; Regan, E. C.; Kleemann, H.; Cai, H.; Shen, Y.; Shinner, M. J.; Sengupta, A.; Watanabe, K.; Taniguchi, T.; Tongay, S.; Zettl, A.; Wang, F. Imaging of Pure Spin-Valley Diffusion Current in WS_2-WSe_2 Heterostructures. *Science* **2018**, *360* (6391), 893−896.

(3) Krishna Kumar, R.; Bandurin, D. A.; Pellegrino, F. M. D.; Cao, Y.; Principi, A.; Guo, H.; Auton, G. H.; Ben Shalom, M.; Ponomarenko, L. A.; Falkovich, G.; Watanabe, K.; Taniguchi, T.; Grigorieva, I. V.; Levitov, L. S.; Polini, M.; Geim, A. K. Superballistic Flow of Viscous Electron Fluid through Graphene Constrictions. *Nat. Phys.* **2017**, *13* (12), 1182−1185.

(4) Bandurin, D. A.; Torre, I.; Kumar, R. K.; Ben Shalom, M.; Tomadin, A.; Principi, A.; Auton, G. H.; Khestanova, E.; Novoselov, K. S.; Grigorieva, I. V.; Ponomarenko, L. A.; Geim, A. K.; Polini, M. Negative Local Resistance Caused by Viscous Electron Backflow in Graphene. *Science* **2016**, *351* (6277), 1055−1058.

(5) Zhao, G.; Han, S.; Wang, A. Z.; Wu, Y. Z.; Zhao, M. W.; Wang, Z. P.; Hao, X. P. Chemical Weathering” Exfoliation of Atom-Thick Transition Metal Dichalcogenides and Their Ultrafast Saturable Absorption Properties. *Adv. Funct. Mater.* **2015**, *25* (33), 5292−5299.

(6) Cho, S.; Kim, S.; Kim, J. H.; Zhao, J.; Seok, J.; Keum, D. H.; Baik, J.; Choe, D.-H.; Chang, K. J.; Suenaga, K.; Kim, S. W.; Lee, Y. H.; Yang, H. Phase Patterning for Ohmic Homojunction Contact in MoTe$_2$. *Science* **2015**, *349* (6248), 625−628.

(7) Rodin, A. S.; Carvalho, A.; Castro Neto, A. H. Strain-Induced Gap Modification in Black Phosphorus. *Phys. Rev. Lett.* **2014**, *112* (17), 176801.

(8) Li, L.; Yu, Y.; Ye, G. J.; Ge, Q.; Ou, X.; Wu, H.; Feng, D.; Chen, X. H.; Zhang, Y. Black Phosphorus Field-Effect Transistors. *Nat. Nanotechnol.* **2014**, *9* (5), 372.

(9) Das, S.; Chen, H.-Y.; Penumatcha, A. V.; Appenzeller, J. High Performance Multilayer MoS$_2$ Transistors with Scandium Contacts. *Nano Lett.* **2013**, *13* (1), 100−105.

(10) Wang, H.; Yu, L.; Lee, Y.-H.; Shi, Y.; Hsu, A.; Chin, M. L.; Li, L.-J.; Dubey, M.; Kong, J.; Palacios, T. Integrated Circuits Based on Bilayer MoS$_2$ Transistors. *Nano Lett.* **2012**, *12* (9), 4674−4680.

(11) Nair, R. R.; Blake, P.; Grigorenko, A. N.; Novoselov, K. S.; Booth, T. J.; Stauber, T.; Peres, N. M.; Geim, A. K. Fine Structure Constant Defines Visual Transparency of Graphene. *Science* **2008**, *320* (5881), 1308−1308.

(12) Meng, Y.; Mao, H.-K.; Eng, P. J.; Trainor, T. P.; Newville, M.; Hu, M. Y.; Kao, C.; Shu, J.; Hausermann, D.; Hemley, R. J. The Formation of sp^3 Bonding in Compressed BN. *Nat. Mater.* **2004**, *3* (2), 111−114.

(13) You, J.; Bongu, S.; Bao, Q.; Panoiu, N. Nonlinear Optical Properties and Applications of 2D Materials: Theoretical and Experimental Aspects. *Nanophotonics* **2018**, *8* (1), 63−97.

(14) Si, M.; Liao, P.-Y.; Qiu, G.; Duan, Y.; Ye, P. D. Ferroelectric Field-Effect Transistors Based on MoS$_2$ and CuInP$_2$S$_6$ Two-Dimensional van der Waals Heterostructure. *ACS Nano* **2018**, *12* (7), 6700−6705.

(15) Zhang, X.; Hou, L.; Ciesielski, A.; Samorì, P. 2D Materials beyond Graphene for High-Performance Energy Storage Applications. *Adv. Energy Mater.* **2016**, *6* (23), 1600671.

(16) Nourbakhsh, A.; Zubair, A.; Sajjad, R. N.; Tavakkoli K. G., A.; Chen, W.; Fang, S.; Ling, X.; Kong, J.; Dresselhaus, M. S.; Kaxiras, E.; Berggren, K. K.; Antoniadis, D.; Palacios, T. MoS$_2$ Field-Effect Transistor with Sub-10 nm Channel Length. *Nano Lett.* **2016**, *16* (12), 7798−7806.

(17) Late, D. J.; Liu, B.; Matte, H. R.; Dravid, V. P.; Rao, C. Hysteresis in Single-Layer MoS$_2$ Field Effect Transistors. *ACS Nano* **2012**, *6* (6), 5635−5641.

(18) Alden, J. S.; Tsen, A. W.; Huang, P. Y.; Hovden, R.; Brown, L.; Park, J.; Muller, D. A.; McEuen, P. L. Strain Solitons and Topological Defects in Bilayer Graphene. *Proc. Natl. Acad. Sci. U. S. A.* **2013**, *110* (28), 11256−11260.

(19) Shimazaki, Y.; Schwartz, I.; Watanabe, K.; Taniguchi, T.; Kroner, M.; Imamoğlu, A. Strongly Correlated Electrons and Hybrid Excitons in A Moiré Heterostructure. *Nature* **2020**, *580* (7804), 472−477.

(20) Balents, L.; Dean, C. R.; Efetov, D. K.; Young, A. F. Superconductivity and Strong Correlations in Moiré Flat Bands. *Nat. Phys.* **2020**, *16*, 725−733.

(21) Yankowitz, M.; Chen, S.; Polshyn, H.; Zhang, Y.; Watanabe, K.; Taniguchi, T.; Graf, D.; Young, A. F.; Dean, C. R. Tuning Superconductivity in Twisted Bilayer Graphene. *Science* **2019**, *363* (6431), 1059−1064.

(22) Cao, Y.; Fatemi, V.; Demir, A.; Fang, S.; Tomarken, S. L.; Luo, J. Y.; Sanchez-Yamagishi, J. D.; Watanabe, K.; Taniguchi, T.; Kaxiras, E.; Ashoori, R. C.; Jarillo-Herrero, P. Correlated Insulator Behaviour at Half-Filling in Magic-Angle Graphene Superlattices. *Nature* **2018**, *556* (7699), 80−84.

(23) Cao, Y.; Fatemi, V.; Fang, S.; Watanabe, K.; Taniguchi, T.; Kaxiras, E.; Jarillo-Herrero, P. Unconventional Superconductivity in Magic-Angle Graphene Superlattices. *Nature* **2018**, *556* (7699), 43−50.

(24) Ni, G.; Wang, H.; Jiang, B.-Y.; Chen, L.; Du, Y.; Sun, Z.; Goldflam, M.; Frenzel, A.; Xie, X.; Fogler, M. Soliton Superlattices in Twisted Hexagonal Boron Nitride. *Nat. Commun.* **2019**, *10*, 4360.

(25) Huang, S.; Kim, K.; Efimkin, D. K.; Lovorn, T.; Taniguchi, T.; Watanabe, K.; MacDonald, A. H.; Tutuc, E.; LeRoy, B. J. Topologically Protected Helical States in Minimally Twisted Bilayer Graphene. *Phys. Rev. Lett.* **2018**, *121* (3), 037702.

(26) Vaezi, A.; Liang, Y.; Ngai, D. H.; Yang, L.; Kim, E.-A. Topological Edge States at A Tilt Boundary in Gated Multilayer Graphene. *Phys. Rev. X* **2013**, *3* (2), 021018.

(27) Hu, G.; Krasnok, A.; Mazor, Y.; Qiu, C.-W.; Alù, A. Moiré Hyperbolic Metasurfaces. *Nano Lett.* **2020**, *20* (5), 3217−3224.

(28) Ni, G. X.; Wang, H.; Wu, J. S.; Fei, Z.; Goldflam, M. D.; Keilmann, F.; Özyilmaz, B.; Castro Neto, A. H.; Xie, X. M.; Fogler, M. M.; Basov, D. N. Plasmons in Graphene Moiré Superlattices. *Nat. Mater.* **2015**, *14* (12), 1217−1222.

(29) Lin, J.; Fang, W.; Zhou, W.; Lupini, A. R.; Idrobo, J. C.; Kong, J.; Pennycook, S. J.; Pantelides, S. T. AC/AB Stacking Boundaries in Bilayer Graphene. *Nano Lett.* **2013**, *13* (7), 3262−3268.

(30) Weston, A.; Zou, Y.; Enaldiev, V.; Summerfield, A.; Clark, N.; Zolyomi, V.; Graham, A.; Yelgel, C.; Magorrian, S.; Zhou, M.; Zultak, J.; Hopkinson, D.; Barinov, A.; Bointon, T. H.; Kretinin, A.; Wilson, N. R.; Beton, P. H.; Fal'ko, V. I.; Haigh, S. J.; Gorbachev, R. Atomic Reconstruction in Twisted Bilayers of Transition Metal Dichalcogenides. *Nat. Nanotechnol.* **2020**, *15*, 592−597.

(31) Rosenberger, M. R.; Chuang, H.-J.; Phillips, M.; Oleshko, V. P.; McCreary, K. M.; Sivaram, S. V.; Hellberg, C. S.; Jonker, B. T. Twist Angle-Dependent Atomic Reconstruction and Moiré Patterns in Transition Metal Dichalcogenide Heterostructures. *ACS Nano* **2020**, *14* (4), 4550−4558.

(32) Yoo, H.; Engelke, R.; Carr, S.; Fang, S.; Zhang, K.; Cazeaux, P.; Sung, S. H.; Hovden, R.; Tsen, A. W.; Taniguchi, T.; Watanabe, K.; Yi, G.-C.; Kim, M.; Luskin, M.; Tadmor, E. B.; Kaxiras, E.; Kim, P. Atomic and Electronic Reconstruction at the van der Waals Interface in Twisted Bilayer Graphene. *Nat. Mater.* **2019**, *18* (5), 448−453.

(33) Naik, M. H.; Jain, M. Ultraflatbands and Shear Solitons in Moiré Patterns of Twisted Bilayer Transition Metal Dichalcogenides. *Phys. Rev. Lett.* **2018**, *121* (26), 266401.

(34) Woods, C. R.; Britnell, L.; Eckmann, A.; Ma, R. S.; Lu, J. C.; Guo, H. M.; Lin, X.; Yu, G. L.; Cao, Y.; Gorbachev, R. V.; Kretinin, A. V.; Park, J.; Ponomarenko, L. A.; Katsnelson, M. I.; Gornostyrev, Y. N.; Watanabe, K.; Taniguchi, T.; Casiraghi, C.; Gao, H-J.; Geim, A. K.; Novoselov, K. S. Commensurate-Incommensurate Transition in Graphene on Hexagonal Boron Nitride. *Nat. Phys.* **2014**, *10* (6), 451−456.

(35) Zhang, Y.; Kim, Y.; Gilbert, M. J.; Mason, N. Electronic Transport in A Two-Dimensional Superlattice Engineered *via* Self-Assembled Nanostructures. *npj 2D Materials and Applications* **2018**, *2*, 31.

(36) Zhang, Y.; Heiranian, M.; Janicek, B.; Budrikis, Z.; Zapperi, S.; Huang, P. Y.; Johnson, H. T.; Aluru, N. R.; Lyding, J. W.; Mason, N. Strain Modulation of Graphene by Nanoscale Substrate Curvatures: A Molecular View. *Nano Lett.* **2018**, *18* (3), 2098−2104.

(37) Hinnefeld, J. H.; Gill, S. T.; Mason, N. Graphene Transport Mediated by Micropatterned Substrates. *Appl. Phys. Lett.* **2018**, *112* (17), 173504.

(38) Carr, S.; Massatt, D.; Torrisi, S. B.; Cazeaux, P.; Luskin, M.; Kaxiras, E. Relaxation and Domain Formation in Incommensurate Two-Dimensional Heterostructures. *Phys. Rev. B: Condens. Matter Mater. Phys.* **2018**, *98* (22), 224102.

(39) Zhang, Y.; Kim, Y.; Gilbert, M. J.; Mason, N. Magnetotransport in A Strain Superlattice of Graphene. *Appl. Phys. Lett.* **2019**, *115* (14), 143508.

(40) Wang, Z.; Wang, Y. B.; Yin, J.; Tovari, E.; Yang, Y.; Lin, L.; Holwill, M.; Birkbeck, J.; Perello, D. J.; Xu, S.; Zultak, J.; Gorbachev, R. V.; Kretinin, A. V.; Taniguchi, T.; Watanabe, K.; Morozov, S. V.; Anđelkovic, M.; Milovanovic, S. P.; Covaci, L.; Peeters, F. M.; Mishchenko, A.; Geim, A. K.; Novoselov, K. S.; Fal'ko, V. I.; Knothe, A.; Woods, C. R. Composite Super-Moiré Lattices in Double-Aligned Graphene Heterostructures. *Science Advances* **2019**, *5* (12), No. eaay8897.

(41) Liu, F.; Wu, W.; Bai, Y.; Chae, S. H.; Li, Q.; Wang, J.; Hone, J.; Zhu, X.-Y. Disassembling 2D van der Waals Crystals into Macroscopic Monolayers and Reassembling into Artificial Lattices. *Science* **2020**, *367* (6480), 903−906.

(42) Chen, Y.-C.; Lin, W.-H.; Tseng, W.-S.; Chen, C.-C.; Rossman, G. R.; Chen, C.-D.; Wu, Y.-S.; Yeh, N.-C. Direct Growth of mm-Size Twisted Bilayer Graphene by Plasma-Enhanced Chemical Vapor Deposition. *Carbon* **2020**, *156*, 212−224.

(43) Kim, K.; DaSilva, A.; Huang, S.; Fallahazad, B.; Larentis, S.; Taniguchi, T.; Watanabe, K.; LeRoy, B. J.; MacDonald, A. H.; Tutuc, E. Tunable Moiré Bands and Strong Correlations in Small-Twist-Angle Bilayer Graphene. *Proc. Natl. Acad. Sci. U. S. A.* **2017**, *114* (13), 3364−3369.

(44) Hsu, W.-T.; Zhao, Z.-A.; Li, L.-J.; Chen, C.-H.; Chiu, M.-H.; Chang, P.-S.; Chou, Y.-C.; Chang, W.-H. Second Harmonic Generation from Artificially Stacked Transition Metal Dichalcogenide Twisted Bilayers. *ACS Nano* **2014**, *8* (3), 2951−2958.

(45) Yuan, L.; Zheng, B.; Kunstmann, J.; Brumme, T.; Kuc, A. B.; Ma, C.; Deng, S.; Blach, D.; Pan, A.; Huang, L. Twist-Angle-Dependent Interlayer Exciton Diffusion in WS_2-WSe_2 Heterobilayers. *Nat. Mater.* **2020**, *19* (6), 617−623.

(46) Tran, K.; Moody, G.; Wu, F.; Lu, X.; Choi, J.; Kim, K.; Rai, A.; Sanchez, D. A.; Quan, J.; Singh, A.; Embley, J.; Zepeda, A.; Campbell, M.; Autry, T.; Taniguchi, T.; Watanabe, K.; Lu, N.; Banerjee, S. K.; Silverman, K. L.; Kim, S.; et al. Evidence for Moiré Excitons in van der Waals Heterostructures. *Nature* **2019**, *567* (7746), 71−75.

(47) Jin, C.; Regan, E. C.; Yan, A.; Iqbal Bakti Utama, M.; Wang, D.; Zhao, S.; Qin, Y.; Yang, S.; Zheng, Z.; Shi, S.; Watanabe, K.; Taniguchi, T.; Tongay, S.; Zettl, A.; Wang, F. Observation of Moiré Excitons in WSe_2/WS_2 Heterostructure Superlattices. *Nature* **2019**, *567* (7746), 76−80.

(48) Hsu, W.-T.; Lin, B.-H.; Lu, L.-S.; Lee, M.-H.; Chu, M.-W.; Li, L.-J.; Yao, W.; Chang, W.-H.; Shih, C.-K. Tailoring Excitonic States of van der Waals Bilayers through Stacking Configuration, Band Alignment, and Valley Spin. *Science Advances* **2019**, *5* (12), No. eaax7407.

(49) Lu, X.; Stepanov, P.; Yang, W.; Xie, M.; Aamir, M. A.; Das, I.; Urgell, C.; Watanabe, K.; Taniguchi, T.; Zhang, G.; Bachtold, A.; MacDonald, A. H.; Efetov, D. K. Superconductors, Orbital Magnets and Correlated States in Magic-Angle Bilayer Graphene. *Nature* **2019**, *574* (7780), 653−657.

(50) Sharpe, A. L.; Fox, E. J.; Barnard, A. W.; Finney, J.; Watanabe, K.; Taniguchi, T.; Kastner, M.; Goldhaber-Gordon, D. Emergent Ferromagnetism near Three-Quarters Filling in Twisted Bilayer Graphene. *Science* **2019**, *365* (6453), 605−608.

(51) Wang, L.; Meric, I.; Huang, P. Y.; Gao, Q.; Gao, Y.; Tran, H.; Taniguchi, T.; Watanabe, K.; Campos, L. M.; Muller, D. A.; Guo, J.; Kim, P.; Hone, J.; Shepard, K. L.; Dean, C. R. One-Dimensional Electrical Contact to A Two-Dimensional Material. *Science* **2013**, *342* (6158), 614−617.

(52) Forsythe, C.; Zhou, X.; Watanabe, K.; Taniguchi, T.; Pasupathy, A.; Moon, P.; Koshino, M.; Kim, P.; Dean, C. R. Band Structure Engineering of 2D Materials Using Patterned Dielectric Superlattices. *Nat. Nanotechnol.* **2018**, *13* (7), 566−571.

(53) Zhang, J.; Wang, J.; Chen, P.; Sun, Y.; Wu, S.; Jia, Z.; Lu, X.; Yu, H.; Chen, W.; Zhu, J.; Xie, G.; Yang, R.; Shi, D.; Xu, X.; Xiang, J.; Liu, K.; Zhang, G. Observation of Strong Interlayer Coupling in MoS_2/WS_2 Heterostructures. *Adv. Mater.* **2016**, *28* (10), 1950−1956.

(54) Mishchenko, A.; Tu, J. S.; Cao, Y.; Gorbachev, R. V.; Wallbank, J. R.; Greenaway, M. T.; Morozov, V. E.; Morozov, S. V.; Zhu, M. J.; Wong, S. L.; Withers, F.; Woods, C. R.; Kim, Y-J.; Watanabe, K.; Taniguchi, T.; Vdovin, E. E.; Makarovsky, O.; Fromhold, T. M.; Fal'ko, V. I.; Geim, A. K.; Eaves, L.; Novoselov, K. S. Twist-Controlled Resonant Tunnelling in Graphene/Boron Nitride/Graphene Heterostructures. *Nat. Nanotechnol.* **2014**, *9* (10), 808−813.

(55) Alexeev, E. M.; Ruiz-Tijerina, D. A.; Danovich, M.; Hamer, M. J.; Terry, D. J.; Nayak, P. K.; Ahn, S.; Pak, S.; Lee, J.; Sohn, J. I.; Molas, M. R.; Koperski, M.; Watanabe, K.; Taniguchi, T.; Novoselov, K. S.; Gorbachev, R. V.; Shin, H. S.; Fal'ko, V. I.; Tartakovskii, A. I. Resonantly Hybridized Excitons in Moiré Superlattices in van der Waals Heterostructures. *Nature* **2019**, *567* (7746), 81−86.

(56) Zhang, Y.; Zhang, Y.; Ji, Q.; Ju, J.; Yuan, H.; Shi, J.; Gao, T.; Ma, D.; Liu, M.; Chen, Y.; Song, X.; Hwang, H. Y.; Cui, Y.; Liu, Z. Controlled Growth of High-Quality Monolayer WS_2 Layers on Sapphire and Imaging Its Grain Boundary. *ACS Nano* **2013**, *7* (10), 8963−8971.

(57) Lee, Y.-H.; Zhang, X.-Q.; Zhang, W.; Chang, M.-T.; Lin, C.-T.; Chang, K.-D.; Yu, Y.-C.; Wang, J. T.-W.; Chang, C.-S.; Li, L.-J.; Lin, T.-W. Synthesis of Large-Area MoS_2 Atomic Layers with Chemical Vapor Deposition. *Adv. Mater.* **2012**, *24* (17), 2320−2325.

(58) Liu, N.; Fu, L.; Dai, B.; Yan, K.; Liu, X.; Zhao, R.; Zhang, Y.; Liu, Z. Universal Segregation Growth Approach to Wafer-Size Graphene from Non-Noble Metals. *Nano Lett.* **2011**, *11* (1), 297−303.

(59) Li, X.; Cai, W.; An, J.; Kim, S.; Nah, J.; Yang, D.; Piner, R.; Velamakanni, A.; Jung, I.; Tutuc, E.; Banerjee, S. K.; Colombo, L.; Ruoff, R. S. Large-Area Synthesis of High-Quality and Uniform Graphene Films on Copper Foils. *Science* **2009**, *324* (5932), 1312−1314.

(60) Li, Y.; Rao, Y.; Mak, K. F.; You, Y.; Wang, S.; Dean, C. R.; Heinz, T. F. Probing Symmetry Properties of Few-Layer MoS_2 and h-BN by Optical Second-Harmonic Generation. *Nano Lett.* **2013**, *13* (7), 3329−3333.

(61) Brotons-Gisbert, M.; Baek, H.; Molina-Sánchez, A.; Campbell, A.; Scerri, E.; White, D.; Watanabe, K.; Taniguchi, T.; Bonato, C.; Gerardot, B. D. Spin-Layer Locking of Interlayer Excitons Trapped in Moiré Potentials. *Nat. Mater.* **2020**, *19* (6), 630−636.

(62) Bai, Y.; Zhou, L.; Wang, J.; Wu, W.; McGilly, L. J.; Halbertal, D.; Lo, C. F. B.; Liu, F.; Ardelean, J.; Rivera, P.; Finney, N. R.; Yang, X.-C.; Basov, D. N.; Yao, W.; Xu, X.; Hone, J.; Pasupathy, A. N.; Zhu, X. Y. Excitons in Strain-Induced One-Dimensional Moiré Potentials at Transition Metal Dichalcogenide Heterojunctions. *Nat. Mater.* **2020**, *19*, 1068−1073.

(63) Li, W.; Lu, X.; Dubey, S.; Devenica, L.; Srivastava, A. Dipolar Interactions between Localized Interlayer Excitons in van der Waals Heterostructures. *Nat. Mater.* **2020**, *19* (6), 624−629.

(64) Seyler, K. L.; Rivera, P.; Yu, H.; Wilson, N. P.; Ray, E. L.; Mandrus, D. G.; Yan, J.; Yao, W.; Xu, X. Signatures of Moiré-Trapped Valley Excitons in $MoSe_2$/WSe_2 Heterobilayers. *Nature* **2019**, *567* (7746), 66−70.

(65) Jin, C.; Regan, E. C.; Wang, D.; Iqbal Bakti Utama, M.; Yang, C.-S.; Cain, J.; Qin, Y.; Shen, Y.; Zheng, Z.; Watanabe, K.; Taniguchi, T.; Tongay, S.; Zettl, A.; Wang, F. Identification of Spin, Valley and Moiré Quasi-Angular Momentum of Interlayer Excitons. *Nat. Phys.* **2019**, *15* (11), 1140−1144.

(66) Okada, M.; Kutana, A.; Kureishi, Y.; Kobayashi, Y.; Saito, Y.; Saito, T.; Watanabe, K.; Taniguchi, T.; Gupta, S.; Miyata, Y.; Yakobson, B. I.; Shinohara, H.; Kitaura, R. Direct and Indirect Interlayer Excitons in A van der Waals Heterostructure of hBN/WS_2/MoS_2/hBN. *ACS Nano* **2018**, *12* (3), 2498−2505.

(67) Gillen, R.; Maultzsch, J. Interlayer Excitons in $MoSe_2$/WSe_2 Heterostructures from First Principles. *Phys. Rev. B: Condens. Matter Mater. Phys.* **2018**, *97* (16), 165306.

(68) Yevtushenko, O. M.; Tsvelik, A. M. Chiral Lattice Supersolid on Edges of Quantum Spin Hall Samples. *Phys. Rev. B: Condens. Matter Mater. Phys.* **2018**, *98* (8), 081118.

(69) Müller, T.; Fölling, S.; Widera, A.; Bloch, I. State Preparation and Dynamics of Ultracold Atoms in Higher Lattice Orbitals. *Phys. Rev. Lett.* **2007**, *99* (20), 200405.

https://doi.org/10.1021/acsnano.0c10435

(70) Sung, J.; Zhou, Y.; Scuri, G.; Zólyomi, V.; Andersen, T. I.; Yoo, H.; Wild, D. S.; Joe, A. Y.; Gelly, R. J.; Heo, H.; Magorrian, S. J.; Bérubé, D.; Valdivia, A. M. M.; Taniguchi, T.; Watanabe, K.; Lukin, M. D.; Kim, P.; Fal'ko, V. I.; Park, H. Broken Mirror Symmetry in Excitonic Response of Reconstructed Domains in Twisted $MoSe_2$/$MoSe_2$ Bilayers. *Nat. Nanotechnol.* **2020**, *15*, 750−754.

(71) Serlin, M.; Tschirhart, C.; Polshyn, H.; Zhang, Y.; Zhu, J.; Watanabe, K.; Taniguchi, T.; Balents, L.; Young, A. Intrinsic Quantized Anomalous Hall Effect in a Moiré Heterostructure. *Science* **2020**, *367* (6480), 900−903.

(72) Shi, H.; Zhan, Z.; Qi, Z.; Huang, K.; Veen, E. V.; Silva-Guillén, J. Á.; Zhang, R.; Li, P.; Xie, K.; Ji, H.; Katsnelson, M. I.; Yuan, S.; Qin, S.; Zhang, Z. Large-Area, Periodic, and Tunable Intrinsic Pseudo-Magnetic Fields in Low-Angle Twisted Bilayer Graphene. *Nat. Commun.* **2020**, *11* (1), 371.

(73) Stewart, G. Unconventional superconductivity. *Adv. Phys.* **2017**, *66* (2), 75−196.

(74) Andrei, E. Y.; MacDonald, A. H. Graphene Bilayers with A Twist. *Nat. Mater.* **2020**, *19* (12), 1265−1275.

(75) Nimbalkar, A.; Kim, H. Opportunities and Challenges in Twisted Bilayer Graphene: A Review. *Nano-Micro Letters* **2020**, *12* (1), 126.

(76) Bistritzer, R.; MacDonald, A. H. Moiré Bands in Twisted Double-Layer Graphene. *Proc. Natl. Acad. Sci. U. S. A.* **2011**, *108* (30), 12233−12237.

(77) Lopes dos Santos, J. M. B.; Peres, N. M. R.; Castro Neto, A. H. Graphene Bilayer with A Twist: Electronic Structure. *Phys. Rev. Lett.* **2007**, *99* (25), 256802.

(78) Cao, Y.; Luo, J.; Fatemi, V.; Fang, S.; Sanchez-Yamagishi, J.; Watanabe, K.; Taniguchi, T.; Kaxiras, E.; Jarillo-Herrero, P. Superlattice-Induced Insulating States and Valley-Protected Orbits in Twisted Bilayer Graphene. *Phys. Rev. Lett.* **2016**, *117* (11), 116804.

(79) Brihuega, I.; Mallet, P.; Gonzalez-Herrero, H.; Trambly de Laissardiere, G.; Ugeda, M. M.; Magaud, L.; Gomez-Rodriguez, J. M.; Yndurain, F.; Veuillen, J.-Y. Unraveling the Intrinsic and Robust Nature of Van Hove Singularities in Twisted Bilayer Graphene by Scanning Tunneling Microscopy and Theoretical Analysis. *Phys. Rev. Lett.* **2012**, *109* (19), 196802.

(80) Luican, A.; Li, G.; Reina, A.; Kong, J.; Nair, R.; Novoselov, K. S.; Geim, A. K.; Andrei, E. Single-Layer Behavior and Its Breakdown in Twisted Graphene Layers. *Phys. Rev. Lett.* **2011**, *106* (12), 126802.

(81) Li, G.; Luican, A.; Lopes dos Santos, J. M. B.; Castro Neto, A. H.; Reina, A.; Kong, J.; Andrei, E. Y. Observation of Van Hove Singularities in Twisted Graphene Layers. *Nat. Phys.* **2010**, *6* (2), 109−113.

(82) Zhang, Y.-H.; Mao, D.; Senthil, T. Twisted Bilayer Graphene Aligned with Hexagonal Boron Nitride: Anomalous Hall Effect and A Lattice Model. *Physical Review Research* **2019**, *1* (3), 033126.

(83) Isobe, H.; Yuan, N. F.; Fu, L. Unconventional Superconductivity and Density Waves in Twisted Bilayer Graphene. *Phys. Rev. X* **2018**, *8* (4), 041041.

(84) Chichinadze, D. V.; Classen, L.; Chubukov, A. V. Nematic Superconductivity in Twisted Bilayer Graphene. *Phys. Rev. B: Condens. Matter Mater. Phys.* **2020**, *101* (22), 224513.

(85) Cao, Y.; Chowdhury, D.; Rodan-Legrain, D.; Rubies-Bigorda, O.; Watanabe, K.; Taniguchi, T.; Senthil, T.; Jarillo-Herrero, P. Strange Metal in Magic-Angle Graphene with Near Planckian Dissipation. *Phys. Rev. Lett.* **2020**, *124* (7), 076801.

(86) Ray, S.; Jung, J.; Das, T. Wannier Pairs in Superconducting Twisted Bilayer Graphene and Related Systems. *Phys. Rev. B: Condens. Matter Mater. Phys.* **2019**, *99* (13), 134515.

(87) Xu, C.; Balents, L. Topological Superconductivity in Twisted Multilayer Graphene. *Phys. Rev. Lett.* **2018**, *121* (8), 087001.

(88) Guo, H.; Zhu, X.; Feng, S.; Scalettar, R. T. Pairing Symmetry of Interacting Fermions on A Twisted Bilayer Graphene Superlattice. *Phys. Rev. B: Condens. Matter Mater. Phys.* **2018**, *97* (23), 235453.

(89) Keimer, B.; Kivelson, S. A.; Norman, M. R.; Uchida, S.; Zaanen, J. From Quantum Matter to High-Temperature Superconductivity in Copper Oxides. *Nature* **2015**, *518* (7538), 179−186.

(90) Lee, P. A.; Nagaosa, N.; Wen, X.-G. Doping A Mott Insulator: Physics of High-Temperature Superconductivity. *Rev. Mod. Phys.* **2006**, *78* (1), 17.

(91) Stepanov, P.; Das, I.; Lu, X.; Fahimniya, A.; Watanabe, K.; Taniguchi, T.; Koppens, F. H.; Lischner, J.; Levitov, L.; Efetov, D. K. Untying the Insulating and Superconducting Orders in Magic-Angle Graphene. *Nature* **2020**, *583*, 375−378.

(92) Saito, Y.; Ge, J.; Watanabe, K.; Taniguchi, T.; Young, A. F. Independent Superconductors and Correlated Insulators in Twisted Bilayer Graphene. *Nat. Phys.* **2020**, *16*, 926−930.

(93) Lian, B.; Wang, Z.; Bernevig, B. A. Twisted Bilayer Graphene: A Phonon-Driven Superconductor. *Phys. Rev. Lett.* **2019**, *122* (25), 257002.

(94) Wu, F.; MacDonald, A.; Martin, I. Theory of Phonon-Mediated Superconductivity in Twisted Bilayer Graphene. *Phys. Rev. Lett.* **2018**, *121* (25), 257001.

(95) Ochi, M.; Koshino, M.; Kuroki, K. Possible Correlated Insulating States in Magic-Angle Twisted Bilayer Graphene under Strongly Competing Interactions. *Phys. Rev. B: Condens. Matter Mater. Phys.* **2018**, *98* (8), 081102.

(96) Xie, Y.; Lian, B.; Jäck, B.; Liu, X.; Chiu, C.-L.; Watanabe, K.; Taniguchi, T.; Bernevig, B. A.; Yazdani, A. Spectroscopic Signatures of Many-Body Correlations in Magic-Angle Twisted Bilayer Graphene. *Nature* **2019**, *572* (7767), 101−105.

(97) Kerelsky, A.; McGilly, L. J.; Kennes, D. M.; Xian, L.; Yankowitz, M.; Chen, S.; Watanabe, K.; Taniguchi, T.; Hone, J.; Dean, C.; Rubio, A.; Pasupathy, A. N. Maximized Electron Interactions at the Magic Angle in Twisted Bilayer Graphene. *Nature* **2019**, *572* (7767), 95−100.

(98) Jiang, Y.; Lai, X.; Watanabe, K.; Taniguchi, T.; Haule, K.; Mao, J.; Andrei, E. Y. Charge Order and Broken Rotational Symmetry in Magic-Angle Twisted Bilayer Graphene. *Nature* **2019**, *573* (7772), 91−95.

(99) Huder, L.; Artaud, A.; Le Quang, T.; de Laissardière, G. T.; Jansen, A. G. M.; Lapertot, G.; Chapelier, C.; Renard, V. T. Electronic Spectrum of Twisted Graphene Layers under Heterostrain. *Phys. Rev. Lett.* **2018**, *120* (15), 156405.

(100) Choi, Y.; Kemmer, J.; Peng, Y.; Thomson, A.; Arora, H.; Polski, R.; Zhang, Y.; Ren, H.; Alicea, J.; Refael, G.; von Oppen, F.; Watanabe, K.; Taniguchi, T.; Nadj-Perge, S. Electronic Correlations in Twisted Bilayer Graphene near the Magic Angle. *Nat. Phys.* **2019**, *15* (11), 1174−1180.

(101) Bi, Z.; Yuan, N. F. Q.; Fu, L. Designing Flat Bands by Strain. *Phys. Rev. B: Condens. Matter Mater. Phys.* **2019**, *100* (3), 035448.

(102) Uri, A.; Grover, S.; Cao, Y.; Crosse, J. A.; Bagani, K.; Rodan-Legrain, D.; Myasoedov, Y.; Watanabe, K.; Taniguchi, T.; Moon, P.; Koshino, M.; Jarillo-Herrero, P.; Zeldov, E. Mapping the Twist-Angle Disorder and Landau Levels in Magic-Angle Graphene. *Nature* **2020**, *581* (7806), 47−52.

(103) Nam, N. N.; Koshino, M. Lattice Relaxation and Energy Band Modulation in Twisted Bilayer Graphene. *Phys. Rev. B: Condens. Matter Mater. Phys.* **2017**, *96* (7), 075311.

(104) Guinea, F.; Walet, N. R. Electrostatic Effects, Band Distortions, and Superconductivity in Twisted Graphene Bilayers. *Proc. Natl. Acad. Sci. U. S. A.* **2018**, *115* (52), 13174−13179.

(105) Jiang, Y.; Anđelković, M.; Milovanović, S. P.; Covaci, L.; Lai, X.; Cao, Y.; Watanabe, K.; Taniguchi, T.; Peeters, F. M.; Geim, A. K.; Andrei, E. Y. Flat Bands in Buckled Graphene Superlattices. *arXiv* **2019**; https://arxiv.org/abs/1904.10147 (accessed March 18, 2021).

(106) Wong, D.; Wang, Y.; Jung, J.; Pezzini, S.; DaSilva, A. M.; Tsai, H.-Z.; Jung, H. S.; Khajeh, R.; Kim, Y.; Lee, J.; Kahn, S.; Tollabimazraehno, S.; Rasool, H.; Watanabe, K.; Taniguchi, T.; Zettl, A.; Adam, S.; MacDonald, A. H.; Crommie, M. F. Local Spectroscopy of Moiré-Induced Electronic Structure in Gate-Tunable Twisted Bilayer Graphene. *Phys. Rev. B: Condens. Matter Mater. Phys.* **2015**, *92* (15), 155409.

(107) Butz, B.; Dolle, C.; Niekiel, F.; Weber, K.; Waldmann, D.; Weber, H. B.; Meyer, B.; Spiecker, E. Dislocations in Bilayer Graphene. *Nature* **2014**, *505* (7484), 533−537.

(108) Uri, A.; Grover, S.; Cao, Y.; Crosse, J. A.; Bagani, K.; Rodan-Legrain, D.; Myasoedov, Y.; Watanabe, K.; Taniguchi, T.; Moon, P.; Koshino, M.; Jarillo-Herrero, P.; Zeldov, E. Mapping the Twist-Angle Disorder and Landau Levels in Magic-Angle Graphene. *Nature* **2020**, *581* (7806), 47−52.

(109) Vasyukov, D.; Anahory, Y.; Embon, L.; Halbertal, D.; Cuppens, J.; Neeman, L.; Finkler, A.; Segev, Y.; Myasoedov, Y.; Rappaport, M. L.; Huber, M. E.; Zeldov, E. A Scanning Superconducting Quantum Interference Device with Single Electron Spin Sensitivity. *Nat. Nanotechnol.* **2013**, *8* (9), 639−644.

(110) Bultinck, N.; Chatterjee, S.; Zaletel, M. P. Mechanism for Anomalous Hall Ferromagnetism in Twisted Bilayer Graphene. *Phys. Rev. Lett.* **2020**, *124* (16), 166601.

(111) Guinea, F.; Katsnelson, M. I.; Geim, A. K. Energy Gaps and A Zero-Field Quantum Hall Effect in Graphene by Strain Engineering. *Nat. Phys.* **2010**, *6* (1), 30−33.

(112) Liu, Y.; Rodrigues, J. N. B.; Luo, Y. Z.; Li, L.; Carvalho, A.; Yang, M.; Laksono, E.; Lu, J.; Bao, Y.; Xu, H.; Tan, S. J. R.; Qiu, Z.; Sow, C. H.; Feng, Y. P.; Neto, A. H. C.; Adam, S.; Lu, J.; Loh, K. P. Tailoring Sample-Wide Pseudo-Magnetic Fields on A Graphene-Black Phosphorus H eterostructure. *Nat. Nanotechnol.* **2018**, *13* (9), 828−834.

(113) Zheng, Z.; Ma, Q.; Bi, Z.; de la Barrera, S.; Liu, M.-H.; Mao, N.; Zhang, Y.; Kiper, N.; Watanabe, K.; Taniguchi, T.; Kong, J.; Tisdale, W. A.; Ashoori, R.; Gedik, N.; Fu, L.; Xu, S.-Y.; Jarillo-Herrero, P. Unconventional Ferroelectricity in Moiré Heterostructures. *Nature* **2020**, *588* (7836), 71−76.

(114) Woods, C. R.; Ares, P.; Nevison-Andrews, H.; Holwill, M. J.; Fabregas, R.; Guinea, F.; Geim, A. K.; Novoselov, K. S.; Walet, N. R.; Fumagalli, L. Charge-Polarized Interfacial Superlattices in Marginally Twisted Hexagonal Boron Nitride. *Nat. Commun.* **2021**, *12*, 347.

(115) Chen, G.; Sharpe, A. L.; Fox, E. J.; Zhang, Y.-H.; Wang, S.; Jiang, L.; Lyu, B.; Li, H.; Watanabe, K.; Taniguchi, T.; Shi, Z.; Senthil, T.; Goldhaber-Gordon, D.; Zhang, Y.; Wang, F. Tunable Correlated Chern Insulator and Ferromagnetism in A Moiré Superlattice. *Nature* **2020**, *579* (7797), 56−61.

(116) Zhang, Y.-H.; Mao, D.; Cao, Y.; Jarillo-Herrero, P.; Senthil, T. Nearly Flat Chern Bands in Moiré Superlattices. *Phys. Rev. B: Condens. Matter Mater. Phys.* **2019**, *99* (7), 075127.

(117) Chittari, B. L.; Chen, G.; Zhang, Y.; Wang, F.; Jung, J. Gate-Tunable Topological Flat Bands in Trilayer Graphene Boron-Nitride Moiré Superlattices. *Phys. Rev. Lett.* **2019**, *122* (1), 016401.

(118) Chen, G.; Sharpe, A. L.; Gallagher, P.; Rosen, I. T.; Fox, E. J.; Jiang, L.; Lyu, B.; Li, H.; Watanabe, K.; Taniguchi, T.; Jung, J.; Shi, Z.; Goldhaber-Gordon, D.; Zhang, Y.; Wang, F. Signatures of Tunable Superconductivity in A Trilayer Graphene Moiré Superlattice. *Nature* **2019**, *572* (7768), 215−219.

(119) Chen, G.; Jiang, L.; Wu, S.; Lyu, B.; Li, H.; Chittari, B. L.; Watanabe, K.; Taniguchi, T.; Shi, Z.; Jung, J.; Zhang, Y.; Wang, F. Evidence of A Gate-Tunable Mott Insulator in A Trilayer Graphene Moiré Superlattice. *Nat. Phys.* **2019**, *15* (3), 237−241.

(120) Shen, C.; Chu, Y.; Wu, Q.; Li, N.; Wang, S.; Zhao, Y.; Tang, J.; Liu, J.; Tian, J.; Watanabe, K.; Taniguchi, T.; Yang, R.; Meng, Z. Y.; Shi, D.; Yazyev, O. V.; Zhang, G. Correlated States in Twisted Double Bilayer Graphene. *Nat. Phys.* **2020**, *16* (5), 520−525.

(121) Liu, X.; Hao, Z.; Khalaf, E.; Lee, J. Y.; Ronen, Y.; Yoo, H.; Haei Najafabadi, D.; Watanabe, K.; Taniguchi, T.; Vishwanath, A.; Kim, P. Tunable Spin-Polarized Correlated States in Twisted Double Bilayer Graphene. *Nature* **2020**, *583*, 221−225.

(122) Li, X.; Wu, F.; Das Sarma, S. Phonon Scattering Induced Carrier Resistivity in Twisted Double-Bilayer Graphene. *Phys. Rev. B: Condens. Matter Mater. Phys.* **2020**, *101* (24), 245436.

(123) Cao, Y.; Rodan-Legrain, D.; Rubies-Bigorda, O.; Park, J. M.; Watanabe, K.; Taniguchi, T.; Jarillo-Herrero, P. Tunable Correlated States and Spin-Polarized Phases in Twisted Bilayer-Bilayer Graphene. *Nature* **2020**, *583*, 215−220.

(124) Burg, G. W.; Zhu, J.; Taniguchi, T.; Watanabe, K.; MacDonald, A. H.; Tutuc, E. Correlated Insulating States in Twisted Double Bilayer Graphene. *Phys. Rev. Lett.* **2019**, *123* (19), 197702.

(125) Tang, Y.; Li, L.; Li, T.; Xu, Y.; Liu, S.; Barmak, K.; Watanabe, K.; Taniguchi, T.; MacDonald, A. H.; Shan, J.; Mak, K. F. Simulation of Hubbard Model Physics in WSe_2/WS_2 Moiré Superlattices. *Nature* **2020**, *579* (7799), 353−358.

(126) Regan, E. C.; Wang, D.; Jin, C.; Bakti Utama, M. I.; Gao, B.; Wei, X.; Zhao, S.; Zhao, W.; Zhang, Z.; Yumigeta, K.; Blei, M.; Carlstrom, J. D.; Watanabe, K.; Taniguchi, T.; Tongay, S.; Crommie, M.; Zettl, A.; Wang, F. Mott and Generalized Wigner Crystal States in WSe_2/WS_2 Moiré Superlattices. *Nature* **2020**, *579* (7799), 359−363.

(127) Zhang, Z.; Wang, Y.; Watanabe, K.; Taniguchi, T.; Ueno, K.; Tutuc, E.; LeRoy, B. J. Flat Bands in Small Angle Twisted Bilayer WSe_2. *Nat. Phys.* **2020**, *16*, 1093−1096.

(128) Wang, L.; Shih, E.-M.; Ghiotto, A.; Xian, L.; Rhodes, D. A.; Tan, C.; Claassen, M.; Kennes, D. M.; Bai, Y.; Kim, B.; Watanabe, K.; Taniguchi, T.; Zhu, X.; Hone, J.; Rubio, A.; Pasupathy, A. N.; Dean, C. R. Correlated Electronic Phases in Twisted Bilayer Transition Metal Dichalcogenides. *Nat. Mater.* **2020**, *19*, 861−866.

(129) Dai, S.; Xiang, Y.; Srolovitz, D. J. Twisted Bilayer Graphene: Moiré with A Twist. *Nano Lett.* **2016**, *16* (9), 5923−5927.

(130) Woźniak, T.; Faria Junior, P. E.; Seifert, G.; Chaves, A.; Kunstmann, J. Exciton g Factors of van der Waals Heterostructures from First-Principles Calculations. *Phys. Rev. B: Condens. Matter Mater. Phys.* **2020**, *101* (23), 235408.

(131) Zhang, K.; Tadmor, E. B. Structural and Electron Diffraction Scaling of Twisted Graphene Bilayers. *J. Mech. Phys. Solids* **2018**, *112*, 225−238.

(132) Holler, J.; Meier, S.; Kempf, M.; Nagler, P.; Watanabe, K.; Taniguchi, T.; Korn, T.; Schuller, C. Low-Frequency Raman Scattering in $WSe_2/MoSe_2$ Heterobilayers: Evidence for Atomic Reconstruction. *Appl. Phys. Lett.* **2020**, *117*, 013104.

(133) Maity, I.; Maiti, P. K.; Krishnamurthy, H.; Jain, M. Reconstruction of Moiré Lattices in Twisted Transition Metal Dichalcogenide Bilayers. *Phys. Rev. B: Condens. Matter Mater. Phys.* **2021**, *103* (12), L121102.

(134) Sushko, A.; De Greve, K.; Andersen, T. I.; Scuri, G.; Zhou, Y.; Sung, J.; Watanabe, K.; Taniguchi, T.; Kim, P.; Park, H. High Resolution Imaging of Reconstructed Domains and Moire Patterns in Functional van der Waals Heterostructure Devices. *arXiv* **2019**; https://arxiv.org/abs/1912.07446 (accessed March 18, 2021).

(135) Luo, Y.; Engelke, R.; Mattheakis, M.; Tamagnone, M.; Carr, S.; Watanabe, K.; Taniguchi, T.; Kaxiras, E.; Kim, P.; Wilson, W. L. *In Situ* Nanoscale Imaging of Moiré Superlattices in Twisted van der Waals Heterostructures. *Nat. Commun.* **2020**, *11*, 4209.

(136) Lin, M.-L.; Tan, Q.-H.; Wu, J.-B.; Chen, X.-S.; Wang, J.-H.; Pan, Y.-H.; Zhang, X.; Cong, X.; Zhang, J.; Ji, W.; Hu, P.-A.; Liu, K.-H.; Tan, P.-H. Moiré Phonons in Twisted Bilayer MoS_2. *ACS Nano* **2018**, *12* (8), 8770−8780.

(137) Puretzky, A. A.; Liang, L.; Li, X.; Xiao, K.; Sumpter, B. G.; Meunier, V.; Geohegan, D. B. Twisted MoSe2 Bilayers with Variable Local Stacking and Interlayer Coupling Revealed by Low-Frequency Raman Spectroscopy. *ACS Nano* **2016**, *10* (2), 2736−2744.

(138) Lui, C. H.; Ye, Z.; Ji, C.; Chiu, K.-C.; Chou, C.-T.; Andersen, T. I.; Means-Shively, C.; Anderson, H.; Wu, J.-M.; Kidd, T.; Lee, Y.-H.; He, R. Observation of Interlayer Phonon Modes in van der Waals Heterostructures. *Phys. Rev. B: Condens. Matter Mater. Phys.* **2015**, *91* (16), 165403.

(139) Enaldiev, V. V.; Zólyomi, V.; Yelgel, C.; Magorrian, S. J.; Fal'ko, V. I. Stacking Domains and Dislocation Networks in Marginally Twisted Bilayers of Transition Metal Dichalcogenides. *Phys. Rev. Lett.* **2020**, *124* (20), 206101.

(140) Andersen, T. I.; Scuri, G.; Sushko, A.; De Greve, K.; Sung, J.; Zhou, Y.; Wild, D. S.; Gelly, R. J.; Heo, H.; Bérubé, D.; Joe, A. Y.; Jauregui, L. A.; Watanabe, K.; Taniguchi, T.; Kim, P.; Park, H.; Lukin, M. D. Excitons in A Reconstructed Moiré Potential in Twisted WSe_2/WSe_2 Homobilayers. *Nat. Mater.* **2021**, DOI: 10.1038/s41563-020-00873-5.

(141) Yankowitz, M.; Jung, J.; Laksono, E.; Leconte, N.; Chittari, B. L.; Watanabe, K.; Taniguchi, T.; Adam, S.; Graf, D.; Dean, C. R.

Dynamic Band-Structure Tuning of Graphene Moiré Superlattices with Pressure. *Nature* **2018**, *557* (7705), 404−408.

(142) Lebedeva, I. V.; Popov, A. M. Commensurate-Incommensurate Phase Transition and A Network of Domain Walls in Bilayer Graphene with A Biaxially Stretched Layer. *Phys. Rev. B: Condens. Matter Mater. Phys.* **2019**, *99* (19), 195448.

(143) Jin, C.; Ma, E. Y.; Karni, O.; Regan, E. C.; Wang, F.; Heinz, T. F. Ultrafast Dynamics in van der Waals Heterostructures. *Nat. Nanotechnol.* **2018**, *13* (11), 994−1003.

(144) Niezborala, C.; Hache, F. Measuring the Dynamics of Circular Dichroism in A Pump-Probe Experiment with A Babinet-Soleil Compensator. *J. Opt. Soc. Am. B* **2006**, *23* (11), 2418−2424.

(145) Franke, K. J.; von Oppen, F. Correlated Insulator by the Slice. *Nat. Phys.* **2020**, *16* (2), 128−129.

(146) Liu, C.-X.; Zhang, S.-C.; Qi, X.-L. The Quantum Anomalous Hall Effect: Theory and Experiment. *Annu. Rev. Condens. Matter Phys.* **2016**, *7* (1), 301−321.

(147) McHenry, M. E.; Laughlin, D. E. Magnetic Properties of Metals and Alloys. *Physical Metallurgy*; Elsevier, 2014; pp 1881−2008.

https://doi.org/10.1021/acsnano.0c10435